

# Transient waves generated by a moving bottom obstacle: a new near-field solution

**Madsen, Per A.; Hansen, Asger Bendix**

*Published in:*
Journal of Fluid Mechanics

*Link to article, DOI:*
10.1017/jfm.2012.54

*Publication date:*
2012

*Document Version*
Publisher's PDF, also known as Version of record

*J. Fluid Mech.* (2012), *vol.* 697, *pp.* 237–272.  
doi:10.1017/jfm.2012.54

# Transient waves generated by a moving bottom obstacle: a new near- eld solution

Per A. Madsen† and Asger Bendix Hansen

Department of Mechanical Engineering, Technical University of Denmark, 2800 Kgs Lyngby, Denmark

(Received 1 July 2011; revised 12 January 2012; accepted 24 January 2012;
first published online 7 March 2012)

We consider the classical problem of a single-layer homogeneous fluid at rest and a low, slowly varying, long and positive bottom obstacle, which is abruptly started from rest to move with a constant speed $V$. As a result a system of transient waves will develop, and we assume that locally in the region over the obstacle dispersion can be ignored while nonlinearity cannot. The relevant governing equations for the near-field solution are therefore the nonlinear shallow water (NSW) equations. These are bidirectional and can be formulated in terms of a two-family system of characteristics. We analytically integrate and eliminate the backward-going family and achieve a versatile unidirectional single-family formulation, which covers subcritical, transcritical and supercritical conditions with relatively high accuracy. The formulation accounts for the temporal and spatial evolution of the bound waves in the vicinity of the obstacle as well as the development of the transient free waves generated at the onset of the motion. At some distance from the obstacle, dispersion starts to play a role and undular bores develop, but up to this point the new formulation agrees very well with numerical simulations based on a high-order Boussinesq formulation. Finally, we derive analytical asymptotic solutions to the new equations, providing estimates of the asymptotic surface levels in the vicinity of the obstacle as well as the crest levels of the leading non-dispersive free waves. These estimates can be used to predict the height and speed of the leading waves in the undular bores. The numerical and analytical solutions to the new single-family formulation of the NSW equations are compared to results based on the forced Korteweg–de Vries/Hopf equation and to numerical Boussinesq simulations.

**Key words:** shallow water flows, solitary waves, waves/free-surface flows

## 1. Introduction

In this work, we consider the classical problem of a single-layer homogeneous fluid at rest and a low, slowly varying, long and positive bottom obstacle, which is abruptly started from rest to move with a constant speed $V$. For simplicity, the flow is assumed to be two-dimensional, and the fluid is inviscid and incompressible. The literature on this problem is rich, and the canonical problem is relevant for river flow over obstacles, stratified flows over sills, airflow over mountain ranges, and to some

† Email address for correspondence: prm@mek.dtu.dk

extent waves generated by fast-going vessels, landslides or shallow water earthquakes. Early studies and observations of single-layer and two-layer flow over obstacles were reported by Long (1954, 1955, 1970, 1972, 1974), Houghton & Kasahara (1968), Houghton & Isaacson (1970), McIntyre (1972), Baines (1977, 1984, 1987), Pratt (1983) and Cole (1985); see also the comprehensive monograph by Baines (1995). In this connection, the formation of shock waves and undular bores is a relevant, interesting and complicated topic in its own right, and theoretical, numerical and experimental contributions have been made by e.g. Favre (1935), Binnie & Orkney (1955), Benjamin & Lighthill (1954), Peregrine (1966) and Gurevich & Pitaevskii (1974).

Houghton & Kasahara (1968) provided a comprehensive asymptotic analysis of the single-layer problem covering subcritical, supercritical and transcritical flow conditions, and capturing the limits of the different flow regimes as well as the asymptotic steady-state surface levels in the bound solution in the vicinity of the obstacle. They assumed hydrostatic pressure (i.e. zero dispersion) throughout the domain, and looked for quasi-steady solutions to the nonlinear shallow water (NSW) equations considering phenomena such as partial blocking, moving hydraulic jumps and rarefaction waves. Their formulation did not cover the temporal and spatial evolution of the bound waves or the transient free waves generated at the onset of the motion.

Grimshaw & Smyth (1986), see also Smyth (1987), made a seminal contribution to the understanding of transcritical flow over a localized but long bottom obstacle. Their approach was dedicated to the case of near-critical or resonant flow, and they applied the forced Korteweg–de Vries equation (fKdV), which incorporates weak dispersion as well as weak nonlinearity and an explicit forcing term representing the moving obstacle. Numerical solutions to the unsteady problem were provided for the case of a positive obstacle as well as for a negative obstacle (i.e. a hole). For a positive obstacle, Grimshaw & Smyth were able to derive explicit analytical solutions to the steady near-field problem. These solutions were obtained by invoking the so-called hydraulic approximation by which the dispersive fKdV equation simplifies to the non-dispersive Hopf equation. The Hopf equation was expressed in terms of a single family of characteristics, and it was analytically integrated to establish the steady (asymptotic) bound solution over the obstacle.

The procedure of Grimshaw & Smyth revealed that a unique feature of transcritical flow is the existence of turning points in some of the characteristic tracks. The asymptotic non-dispersive solutions upstream and downstream of the crest of the obstacle were determined by characteristics starting from the critical turning point, which separated the cluster of turning characteristics from the non-turning ones. The resulting near-field solution incorporated an upstream/downstream setup/setdown and discrete shock waves (hydraulic jumps) moving ahead of/behind the obstacle. With the non-dispersive solution at hand, Grimshaw & Smyth then replaced the idealized shock waves by dispersive undular bores consisting of modulated cnoidal wave trains. In this connection they generalized the formulation by Gurevich & Pitaevskii (1974) to cover the unsteady upstream and downstream bores evolving in the transcritical far-field solution.

The work by Grimshaw & Smyth (1986) provided a profound understanding of the physical mechanisms associated with transcritical flow, an elegant analytical determination of the non-dispersive bound waves in the vicinity of the obstacle, and relatively simple asymptotic expressions for the surface levels and celerities of the upstream and downstream bores. As such their formulation was much more rich and detailed than the asymptotic steady-state NSW formulation by Houghton &

Kasahara (1968). On the other hand, it should also be acknowledged that the forced KdV and Hopf equations have their limitations, which will be summarized in the following. First, let us consider the classical unidirectional KdV equation. This can be derived on the basis of the classical bidirectional Boussinesq equations (e.g. Peregrine 1967) utilizing the scaling of $\varepsilon = O(\mu^2)$, where $\varepsilon$ defines the nonlinearity and $\mu$ the dispersion. In this process, we assume that waves are moving in a single direction only. Note, however, that even if the intention is to derive the KdV equation in a fixed frame of reference, it is necessary as part of the procedure to shift to a coordinate system moving with the unknown wave celerity $c$, i.e. to shift to $X = ct - x$ and $\tau = \varepsilon t$. In this coordinate system only slow time variations are considered, and it turns out that we need to assume that $(c - c_0)/c_0 = O(\varepsilon)$, where $c_0$ is the linear shallow water celerity. Once the necessary manipulations are made, we can shift back to a fixed coordinate system, but the underlying restriction on the magnitude of $c$ is still valid. Second, let us consider the forced KdV equation for the case of a bottom obstacle moving with constant speed $V$. This can also be derived on the basis of the classical bidirectional Boussinesq equations allowing for an implicit time-varying bottom. The procedure follows rather closely the standard KdV derivation except that this time we need to assume that $(V - c_0)/c_0 = O(\varepsilon)$. This restriction implies that the equations are formally valid only for near-critical flow and not valid for e.g. subcritical and supercritical flow. In addition to this restriction on the speed of the bottom obstacle, it turns out that we also formally need to assume that the relative height of the obstacle is one order smaller than the surface elevation, which again is one order smaller than the water depth (see §§ 3 and 4).

With these restrictions in accuracy and application, it would be attractive, if possible, to extend the hydraulic method by Grimshaw & Smyth from the fKdV/Hopf formulation to a Boussinesq/NSW formulation. One severe problem, in this connection, is that the NSW equations are bidirectional and lead to a two-family system of characteristics, which need to intersect and exchange information in contrast to the unidirectional Hopf equation. This is not a big problem in the subcritical and supercritical flow regime, but in the transcritical regime the appearance of turning points makes it very difficult, if not impossible, to keep track of the intersections of the two families of characteristics.

In this work, we derive a new single-family characteristic formulation of the NSW equations. This is achieved by analytically integrating and eliminating the other family of characteristics, and as a result we derive an equation which is as versatile as the Hopf equation and as accurate as the NSW equations. This formulation provides an accurate temporal and spatial evolution of the transient waves up to the point where dispersion becomes important. The formulation is analytically integrated to provide asymptotic expressions for the upstream and downstream levels of the bound and free waves. Section 2 provides a brief summary of the classical steady-state theory by Houghton & Kasahara (1968). Section 3 covers the derivation of the new single-family NSW formulation, which allows an accurate determination of the non-dispersive transient waves. Section 4 covers the analytical integration of the new equations resulting in simple (but approximate) expressions for the asymptotic levels of the bound and free waves. In this section we also discuss the concepts of turning points, the limiting characteristic, the crest characteristic, caustics and the classification of flow regimes. Section 5 provides a brief discussion of the formation of shock waves and undular bores with emphasis on simple estimates of the speed of the leading and trailing edges. Section 6 covers numerical results and a comparison with a high-order Boussinesq model for various flow regimes. We conduct a systematic verification

of the temporal and spatial evolution of the bound and free waves, and verify the asymptotic levels estimated by the new theory. Finally, § 7 contains the summary and conclusions.

## 2. The NSW equations and the classical steady-state solution

We consider a low, slowly varying, long and positive bottom obstacle, which is abruptly started from rest to move with a constant speed in initially calm water. The fluid is assumed to be inviscid and incompressible, and we assume the pressure to be hydrostatic throughout the domain, ignoring dispersion but allowing for nonlinear effects. This leads to the unsteady NSW equations. Houghton & Kasahara (1968) considered these equations from a frame of reference moving with the obstacle, and they derived an asymptotic steady-state solution for the bound waves in the vicinity of the obstacle, while ignoring the forward-going and backward-going free waves. In the following we provide a summary of their solution.

### 2.1. *The governing equations*

In a dimensional fixed frame of reference ($x^*$, $t^*$), the NSW equations can be expressed as

$$\frac{\partial d^*}{\partial t^*} + \frac{\partial}{\partial x^*}(U^* d^*) = 0, \tag{2.1}$$

$$\frac{\partial U^*}{\partial t^*} + U^* \frac{\partial U^*}{\partial x^*} + g \frac{\partial \eta^*}{\partial x^*} = 0, \tag{2.2}$$

where $U^*$ is the flow velocity, $\eta^*$ is the surface elevation measured from the horizontal still water level, $d^*$ is the local water depth including the effect of the moving bottom obstacle, and $g$ is the acceleration due to gravity. This water depth can be expressed as

$$d^* = h_0^* + \eta^* - \Gamma^*, \tag{2.3}$$

where $h_0^*$ is the constant still water depth, and $\Gamma^*$ defines the localized bottom obstacle measured from the undisturbed flat sea bottom and moving with the constant speed $V^*$. Throughout this paper we consider the following specific shape of the bottom obstacle:

$$\Gamma^*[x^*, t^*] = \frac{\Gamma_m^*}{2}\left(1 + \cos\left[2\pi\left(\frac{V^* t^* - x^*}{L^*}\right)\right]\right) \quad \text{for } -\frac{1}{2} \leqslant \frac{V^* t^* - x^*}{L^*} \leqslant \frac{1}{2}, \tag{2.4}$$

where $\Gamma_m^* > 0$ is the maximum positive height of the obstacle and $L^*$ is the width of the obstacle. For $|V^* t^* - x^*| \geqslant L^*/2$ we have that $\Gamma^* = 0$, and the bottom is horizontal.

We non-dimensionalize all variables by the still water depth $h_0^*$ and the linear shallow water celerity $c_0^* \equiv \sqrt{g h_0^*}$ as follows:

$$\eta \equiv \frac{\eta^*}{h_0^*}, \quad d \equiv \frac{d^*}{h_0^*}, \quad \Gamma \equiv \frac{\Gamma^*}{h_0^*}, \quad x \equiv \frac{x^*}{h_0^*}, \tag{2.5}$$

$$V \equiv \frac{V^*}{c_0^*}, \quad U \equiv \frac{U^*}{c_0^*}, \quad c \equiv \frac{c^*}{c_0^*}, \quad \tau \equiv \frac{c_0^*}{h_0^*} t^*, \tag{2.6}$$

and furthermore, we introduce the moving frame of reference $\chi$ and the associated flow velocity $U_m$ defined by

$$\chi \equiv \tau V - x \quad \text{and} \quad U_m \equiv V - U. \tag{2.7}$$

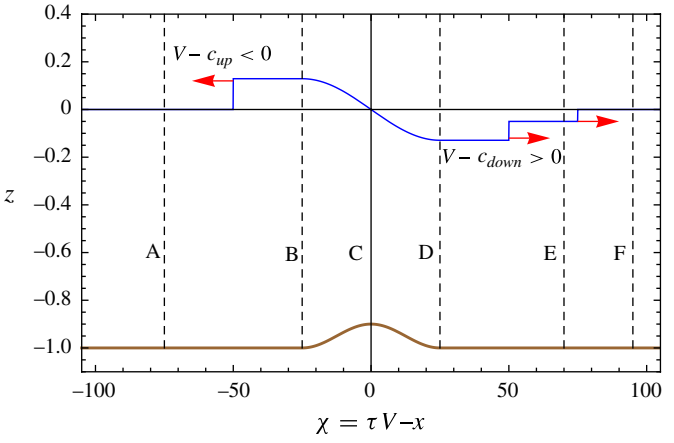


FIGURE 1. (Colour online available at journals.cambridge.org/flm) Definition sketch of transcritical flow in connection with a moving bottom obstacle. The coordinate system is moving with the obstacle, and the upstream/downstream regions correspond to negative/positive values of $\chi$.

Within the moving coordinate system $(\chi, \tau)$, the bottom obstacle is described as $\Gamma[\chi]$ and the governing equations (2.1)–(2.2) read

$$\frac{\partial \eta}{\partial \tau} + \frac{\partial}{\partial \chi}(U_m d) = 0, \quad \frac{\partial U_m}{\partial \tau} + \frac{\partial}{\partial \chi}\left(\frac{U_m^2}{2} + \eta\right) = 0. \tag{2.8}$$

### 2.2. *Subcritical and supercritical solutions*

Let us first consider the case of subcritical or supercritical flow conditions throughout the domain, and look for steady-state solutions to (2.8). By utilizing the far-field conditions $U = 0$, $\eta = 0$ and $d = 1$ , this leads to the conservation equations

$$d(V - U) = V \quad \text{and} \quad \eta + \frac{(V - U)^2}{2} = \frac{V^2}{2}, \tag{2.9}$$

where $d = 1 + \eta - \Gamma$. Conditions at cross-section C located at the crest of the moving obstacle (see figure 1) are of special interest, and the Froude number (in the moving frame) at this location is defined by

$$\mathscr{F}_C \equiv \frac{V - U_C}{\sqrt{d_C}}. \tag{2.10}$$

Whenever $\mathscr{F}_C \to 1$, we reach critical conditions at the crest of the obstacle, and in this case a combination of (2.9) and (2.10) leads to $d_C = V^{2/3}$, and

$$\Gamma_m = 1 + \tfrac{1}{2}V^2 - \tfrac{3}{2}V^{2/3}. \tag{2.11}$$

This defines the NSW transition from subcritical to transcritical flow ($V_{low}$) and from transcritical to supercritical flow ($V_{high}$).

### 2.3. *Transcritical solutions*

In the case of transcritical flow conditions over the submerged obstacle, an upstream shock wave will move ahead of the bar with speed $c_{up}$, while a downstream shock

wave will fall behind the bar with speed $c_{down}$. In a fixed frame both shock waves will move in the direction of the obstacle so that

$$c_{up} > V > c_{down}, \tag{2.12}$$

but in the moving $(\chi, \tau)$ frame, the upstream shock will move to the left with the relative speed of $V - c_{up} < 0$, while the downstream shock will move to the right with the relative speed of $V - c_{down} > 0$. As shown in figure 1, we can now divide the domain into six cross-sections: A, far ahead of the upstream shock in completely calm conditions; B, at the upstream toe of the obstacle, which is assumed to be behind the upstream bore; C, at the crest of the obstacle; D, at the downstream toe of the obstacle, which is assumed to be in front of the downstream bore; E, immediately downstream of the downstream bore; F, far downstream in completely calm conditions.

2.3.1. *The asymptotic upstream problem*

The first step is to conserve mass and momentum between sections A and B, and for this purpose it is convenient to use a coordinate system moving with the upstream shock celerity $c_{up}$. Within this frame we can apply the steady-state jump conditions

$$d_B(c_{up} - U_B) = d_A(c_{up} - U_A) \quad \text{and} \quad c_{up} = U_A + \sqrt{\frac{d_B(d_A + d_B)}{2d_A}} > 0, \tag{2.13}$$

where $d_A = 1$, $U_A = 0$ and $d_B = 1 + \eta_B$. Next, mass and energy should be conserved between sections $B$ and $C$, and for this purpose we apply a coordinate system moving with $V$. This yields

$$d_B(V - U_B) = d_C(V - U_C) \quad \text{and} \quad \eta_B + \frac{(V - U_B)^2}{2} = \eta_C + \frac{(V - U_C)^2}{2}, \tag{2.14}$$

where $d_C = 1 + \eta_C - \Gamma_m$. Finally, we utilize that throughout transcritical conditions, the Froude number at section $C$ will be unity, i.e. $\mathscr{F}_C = 1$. This gives us five equations with the five unknowns $\eta_B$, $U_B$, $\eta_C$, $U_C$ and $c_{up}$, by which the asymptotic upstream problem is fully closed and solvable.

2.3.2. *The asymptotic downstream problem*

In accordance with figure 1, we first assume that the downstream bore will be located in the flat region behind the downstream toe of the obstacle. In this case supercritical conditions will govern from section C to D, and the steady-state conservation of mass and energy in the frame moving with $V$ can be expressed as

$$d_D(V - U_D) = d_C(V - U_C) \quad \text{and} \quad \eta_D + \frac{(V - U_D)^2}{2} = \eta_C + \frac{(V - U_C)^2}{2}, \tag{2.15}$$

where $d_D = 1 + \eta_D$. Notice that (2.15) is formally identical to (2.14), hence we need to add the additional requirement $\mathscr{F}_B < \mathscr{F}_C = 1 < \mathscr{F}_D$, in order to obtain the correct solutions in sections B and D. All three Froude numbers are defined in the frame moving with the speed $V$. The matching of sections D and E is similar to the previous matching between sections A and B except that this time the frame is moving with $c_{down}$. Within this moving frame, the steady-state conservation of mass and momentum leads to the jump conditions,

$$d_D(c_{down} - U_D) = d_E(c_{down} - U_E) \quad \text{and} \quad c_{down} = U_D + \sqrt{\frac{d_E(d_D + d_E)}{2d_D}} > 0, \tag{2.16}$$

where $d_E = 1 + \eta_E$.

Finally, Houghton & Kasahara (1968) connected sections E and F by the rarefaction condition

$$V - U_E - 2\sqrt{d_E} = V - U_F - 2\sqrt{d_F}, \tag{2.17}$$

where $d_F = 1$ and $U_F = 0$. This gives us five new equations with the five unknowns $\eta_D$, $U_D$, $\eta_E$, $U_E$ and $c_{down}$, by which the asymptotic downstream problem is closed and solvable.

It should be emphasized that this downstream solution requires that $c_{down} < V$, i.e. that the downstream bore is detached from the moving obstacle. When $c_{down} = V$, the downstream bore will catch up with the moving obstacle and become attached with a jump occurring somewhere on the sloping bottom between sections $C$ and $D$. Houghton & Kasahara (1968) assumed that the jump was an abrupt and local phenomenon with the front and back located at the same $\chi$ position. On this basis they established a system of seven equations with seven unknowns for this special problem.

## 3. A new characteristic formulation of the unsteady NSW equations

The abrupt onset of the motion of the obstacle will generate a series of transient waves moving in the upstream and downstream directions. In order to cover the temporal and spatial evolution of these waves, we need unsteady differential equations incorporating nonlinearity as well as dispersion. Grimshaw & Smyth (1986) applied the forced KdV equation, which incorporates weak dispersion as well as weak nonlinearity and an explicit forcing term representing the moving obstacle. In addition to numerical simulations, their work concentrated on analytical solutions. For this purpose, they divided the problem into a non-dispersive near-field solution covering the vicinity of the obstacle, and a dispersive far-field solution covering the upstream and downstream undular bores. In the near field, the dispersive fKdV equation was simplified to the non-dispersive Hopf equation, which was solved by the method of characteristics to provide the bound solution over the obstacle. As a step up in accuracy, various Boussinesq formulations are available, e.g. Peregrine (1967), Su & Gardner (1969), Madsen & Sørensen (1992), Nwogu (1993), and Madsen, Bingham & Liu (2002) and Madsen, Bingham & Schäffer (2003), and despite their very different levels of sophistication and accuracy with respect to dispersion and deep water capacities, they all simplify to the NSW equations in the dispersion-free shallow water limit.

In this section we shall pursue characteristic solutions to the unsteady NSW equations with the objective of establishing a new unidirectional single-family formulation of the equations.

### 3.1. *The classical characteristic formulation of the NSW equations*

First, we derive the classical characteristic form of the NSW equations, which we denote the MOC (methods of characteristics) formulation. The first step is to introduce the celerity $c$ defined by

$$c^2 = d \quad \text{where } d(\chi, \tau) = 1 + \eta(\chi, \tau) - \Gamma(\chi). \tag{3.1}$$

Differentiation of (3.1) now yields

$$2c\frac{\partial c}{\partial \chi} = \frac{\partial d}{\partial \chi} = \left(\frac{\partial \eta}{\partial \chi} - \frac{\partial \Gamma}{\partial \chi}\right) \quad \text{and} \quad 2c\frac{\partial c}{\partial \tau} = \frac{\partial d}{\partial \tau} = \frac{\partial \eta}{\partial \tau}. \tag{3.2}$$

Next, we substitute this into the governing equations (2.8) to obtain

$$2\frac{\partial c}{\partial \tau} + 2U_m\frac{\partial c}{\partial \chi} + c\frac{\partial U_m}{\partial \chi} = 0, \tag{3.3}$$

$$\frac{\partial U_m}{\partial \tau} + U_m\frac{\partial U_m}{\partial \chi} + 2c\frac{\partial c}{\partial \chi} + \frac{\partial \Gamma}{\partial \chi} = 0. \tag{3.4}$$

Adding and subtracting (3.3)–(3.4), now leads to the classical characteristic formulation of the NSW equations seen from the moving coordinate system

$$\frac{\mathrm{D}R_\pm}{\mathrm{D}\tau} \equiv \frac{\partial R_\pm}{\partial \tau} + \frac{\mathrm{d}\chi_\pm}{\mathrm{d}\tau}\frac{\partial R_\pm}{\partial \chi_\pm} = -\frac{\partial \Gamma}{\partial \chi_\pm}, \tag{3.5}$$

where

$$R_\pm \equiv U_m \pm 2c = V - U \pm 2c, \tag{3.6}$$

$$\frac{\mathrm{d}\chi_\pm}{\mathrm{d}\tau} \equiv U_m \pm c = V - U \pm c. \tag{3.7}$$

This is a two-family (bidirectional) set of characteristics, which need to intersect and exchange information concerning the local values of $R_+$ and $R_-$ during the solution procedure. Both variables are necessary in order to determine the local values of $c$ and $U$, and according to (3.6) we get

$$V - U = \tfrac{1}{2}(R_+ + R_-), \quad c = \tfrac{1}{4}(R_+ - R_-). \tag{3.8}$$

It should be emphasized, that the $\chi_+(\tau)$ characteristics move in the opposite direction to the obstacle (negative $x$-direction for positive $V$, which corresponds to the positive $\chi$-direction), and they basically take care of the downstream-propagating free wave. In contrast the $\chi_-(\tau)$ characteristics move in the same direction as the obstacle (positive $x$-direction for positive $V$), and they basically take care of the upstream-propagating free wave. Seen from the moving coordinate system, $\chi_-(\tau)$ will move in the negative $\chi$-direction (ahead of the obstacle) for subcritical conditions, and in the positive $\chi$-direction (falling behind the obstacle) for supercritical conditions.

For subcritical and supercritical flow conditions, it is straightforward to solve (3.5)–(3.8) numerically by tracking and intersecting the two families of characteristics even though shock waves may form in the upstream or downstream free waves. However, for transcritical flow conditions, the tracking procedure becomes very complicated because the $\chi_-(\tau)$ characteristics will experience turning points over the obstacle. In this case the MOC method is inconvenient for practical solutions.

### 3.2. *Analytical integration of the $\chi_+(\tau)$ characteristics*

The non-dispersive Hopf equation, applied by Grimshaw & Smyth (1986) in the vicinity of the moving obstacle, provides an attractive and convenient formulation for transcritical flow, because it consists of a single family (unidirectional) of characteristics with the $U$ variable having already been eliminated during the derivation of the original KdV equation. The single family of characteristics imbedded in the Hopf equation corresponds to the $\chi_-(\tau)$ characteristics of the NSW equations, and it is this family which will experience turning points and local shock waves on both sides of the hump in the case of transcritical flow. In the following, we shall pursue an approximative NSW formulation, which reduces the classical two-family system to a single $\chi_-(\tau)$ family. This calls for an analytical integration of the $\chi_+(\tau)$ characteristics by which the velocity $U$ can be approximated by an analytical expression.

3.2.1. *A new approximation for U*

According to (3.5)–(3.7), the $R_+$ characteristics are governed by

$$\frac{\partial R_+}{\partial \tau} + \frac{\mathrm{d}\chi_+}{\mathrm{d}\tau}\frac{\partial R_+}{\partial \chi_+} = -\frac{\partial \Gamma}{\partial \chi_+}, \tag{3.9}$$

where

$$R_+ \equiv V - U + 2c \quad \text{and} \quad \frac{\mathrm{d}\chi_+}{\mathrm{d}\tau} \equiv V - U + c. \tag{3.10}$$

In the following derivation, we formally assume that

$$\eta = O(\varepsilon), \quad U = O(\varepsilon), \quad \Gamma = O(\varepsilon) \quad \text{with } \varepsilon < 1, \tag{3.11}$$

which implies that

$$d = 1 + \varepsilon\,(\eta - \Gamma)\,, \tag{3.12}$$

and

$$c \equiv \sqrt{d} \simeq 1 + \frac{\varepsilon}{2}\,(\eta - \Gamma) + O(\varepsilon^2). \tag{3.13}$$

Note that the explicit $\varepsilon$ factor has been included to indicate the order of magnitude of the different terms. Actually, we do not intend to replace $c$ by (3.13), but merely utilize that

$$c - 1 = O(\varepsilon). \tag{3.14}$$

By introducing (3.11) and (3.14) into (3.10) we obtain

$$R_+ = V + 2 + \varepsilon\,(2(c-1) - U)\,, \tag{3.15}$$

$$\frac{\mathrm{d}\chi_+}{\mathrm{d}\tau} = V + 1 + \varepsilon\,(c - 1 - U)\,. \tag{3.16}$$

The leading-order terms in (3.15) are constants, hence they do not influence the result and may be excluded from $R_+$. Next, we insert (3.15)–(3.16) into (3.9) and collect terms of $O(\varepsilon)$ to obtain

$$\varepsilon\frac{\partial}{\partial \tau}\,(2(c-1) - U) + \varepsilon\,(V+1)\,\frac{\partial}{\partial \chi_+}\,(2(c-1) - U) + \varepsilon\frac{\partial \Gamma}{\partial \chi_+} = O(\varepsilon^2). \tag{3.17}$$

Notice that the consequence of ignoring the $\varepsilon^2$-terms in (3.17) is that the characteristic tracks $\chi_+(\tau)$ will be approximated by

$$\frac{\mathrm{d}\chi_+}{\mathrm{d}\tau} \simeq V + 1, \quad \text{i.e.} \quad \chi_+(\tau) \simeq \chi_+(0) + \tau(V+1). \tag{3.18}$$

This implies that the $\chi_+(\tau)$ tracks are assumed to be straight and independent of the intersections with the $\chi_-(\tau)$ characteristics, and this is a really important simplification of the procedure.

Next, we utilize that $\Gamma$ is a function of $\chi_+(\tau)$ but not explicitly of $\tau$, and this allows the following manipulations

$$\varepsilon\frac{\mathrm{D}}{\mathrm{D}\tau}\left(\frac{\Gamma}{V+1}\right) = \varepsilon\,(V+1)\,\frac{\partial}{\partial \chi_+}\left(\frac{\Gamma}{V+1}\right) + O(\varepsilon^2) = \varepsilon\frac{\partial \Gamma}{\partial \chi_+} + O(\varepsilon^2). \tag{3.19}$$

By inserting (3.19) into (3.17) we finally obtain

$$\varepsilon \frac{\mathrm{D}}{\mathrm{D}\tau}\left(2(c-1)-U+\frac{\Gamma}{V+1}\right)=O(\varepsilon^2), \tag{3.20}$$

which defines the approximative conservation equation for the $\chi_+$ characteristics.

It is now straightforward to integrate (3.20) along $\chi_+(\tau)$ starting from $\chi_+(0)$, and in this process we utilize the starting conditions

$$\eta[\chi_+(0)]=0, \quad d[\chi_+(0)]=1-\Gamma[\chi_+(0)], \tag{3.21}$$

$$U[\chi_+(0)]=0, \quad c[\chi_+(0)]=\sqrt{1-\Gamma[\chi_+(0)]}. \tag{3.22}$$

Consequently, the integration of (3.20) leads to the important result

$$U[\chi_+(\tau)]=2\left(c[\chi_+(\tau)]-1\right)+\widetilde{\alpha}, \tag{3.23}$$

where

$$\widetilde{\alpha}\equiv 2-2\sqrt{1-\Gamma[\chi_+(0)]}+\left(\frac{\Gamma[\chi_+(\tau)]-\Gamma[\chi_+(0)]}{V+1}\right). \tag{3.24}$$

Notice that (3.23)–(3.24) incorporate a memory effect by utilizing information related to $\chi_+(0)$, i.e. from the location where the characteristics started at $\tau=0$.

3.2.2. *Similar approximations from the literature*

Baines (1995), in his § 2.3, argued that 'the downstream-propagating wave is generally little affected by nonlinearities, but travels quickly downstream away from the vicinity of the obstacle. Whilst necessary to satisfy the initial conditions, these waves are unimportant otherwise, and on the upstream side of the obstacle, the equations for the variables on this same family of characteristics may be integrated to yield'

$$U=2(c-1). \tag{3.25}$$

We note that this is actually the classical expression for simple waves travelling into undisturbed waters, and obviously (3.23) simplifies to (3.25) as long as the $\chi_+(\tau)$ characteristics stay completely away from the obstacle, i.e. with $\widetilde{\alpha}=0$.

It should also be mentioned that El, Grimshaw & Smyth (2009) modified Houghton & Kasahara's (1968) steady-state formulation, which was summarized in § 2.3. Firstly, they replaced the upstream and downstream shock conditions by undular jump conditions by which e.g. (2.16) was simplified to

$$V-U_D+2\sqrt{d_D}=V-U_E+2\sqrt{d_E}. \tag{3.26}$$

Secondly, they showed that the downstream Riemann invariant could be ignored for sufficiently small topographic amplitudes, and this corresponded to ignoring the rarefaction condition (2.17), while using the relation (3.25), i.e.

$$U_E=2\left(\sqrt{d_E}-1\right). \tag{3.27}$$

By combining these two equations, they could replace (2.16)–(2.17) by

$$V-U_D+2\sqrt{d_D}=V+2. \tag{3.28}$$

Finally, let us discuss the approximation imbedded in the KdV and Hopf formulations considered by Grimshaw & Smyth (1986). This corresponds to a global

use of (3.25), and requires that the scalings from (3.11) are modified to

$$\eta = O(\varepsilon), \quad U = O(\varepsilon), \quad \Gamma = O(\varepsilon^2) \quad \text{with } \varepsilon < 1. \tag{3.29}$$

Hence we need to assume that the height of the obstacle is one order of magnitude smaller than the surface elevation, which again is one order smaller than the depth. In this case (3.23) simplifies to (3.25). If we then additionally insert (3.13) into (3.25), the velocity further simplifies to

$$U = \eta. \tag{3.30}$$

### 3.3. *A single-family characteristic formulation of the NSW equations*

#### 3.3.1. *The new AMOC formulation*

Having established an analytical estimate of the velocity in (3.23), we are now able to formulate the NSW equations in terms of a single family of characteristics. Being an approximative formulation, we call this the AMOC (approximative method of characteristics) formulation of the NSW equations. According to (3.5)–(3.7), the $\chi_-$ characteristics are governed by

$$\frac{\partial R_-}{\partial \tau} + \frac{\mathrm{d}\chi_-}{\mathrm{d}\tau}\frac{\partial R_-}{\partial \chi_-} = -\frac{\partial \Gamma}{\partial \chi_-}, \tag{3.31}$$

where

$$R_- \equiv V - U - 2c \quad \text{and} \quad \frac{\mathrm{d}\chi_-}{\mathrm{d}\tau} \equiv V - U - c. \tag{3.32}$$

At any $\chi_-(\tau)$ location, we would now like to pass on the information about $U$ from the intersecting $\chi_+(\tau)$ system. In principle this information is available in (3.23), but we need to track the location of $\chi_+(0)$ for any choice of $\chi_-(\tau) = \chi_+(\tau)$. Conveniently, this back-tracing is greatly simplified by (3.18), which leads to the approximation

$$\chi_+(0) \simeq \chi_-(\tau) - \tau(V + 1). \tag{3.33}$$

Consequently, we can express the velocity $U$ along the $\chi_-(\tau)$ characteristics as

$$U = 2(c - 1) + \alpha, \tag{3.34}$$

where

$$\alpha \equiv 2 - 2\sqrt{1 - \Gamma[\chi_-(\tau) - \tau(V + 1)]} + \left(\frac{\Gamma[\chi_-(\tau)] - \Gamma[\chi_-(\tau) - \tau(V + 1)]}{V + 1}\right). \tag{3.35}$$

Notice that $\alpha$ depends not only on the position $\chi_-(\tau)$, but also explicitly on the time $\tau$ due to the memory feature of $\chi_+(0)$.

Two situations are of special interest: the first one is the initial condition for $\tau = 0$, in which case (3.35) simplifies to

$$\alpha_0 = 2 - 2\sqrt{1 - \Gamma[\chi_-(0)]}. \tag{3.36}$$

The second one is for large values of $\tau$, where the back-tracing to $\chi_+(0)$ typically ends in the flat region surrounding the moving obstacle. If we select, for example, the location $\chi_-(\tau) = 0$, the time it takes to back-trace to the flat surrounding region is $\tau_1 = L/(2V + 2)$. Hence, asymptotically (3.35) simplifies to

$$\alpha_\infty \equiv \frac{\Gamma[\chi_-(\tau)]}{V + 1}. \tag{3.37}$$

Next, we insert (3.34) in (3.32) to obtain

$$R_- = V - 2 - 4(c-1) - \alpha, \tag{3.38}$$

$$\frac{\mathrm{d}\chi_-}{\mathrm{d}\tau} = V - 1 - 3(c-1) - \alpha. \tag{3.39}$$

Again there is no reason to keep the first two constant terms in $R_-$, and we replace it by the alternative Riemann invariant

$$R \equiv 4\,(c-1) + \alpha. \tag{3.40}$$

In terms of $R$, the new single-family AMOC formulation of the NSW equations now reads

$$\frac{\mathrm{D}R}{\mathrm{D}\tau} = \frac{\partial \Gamma}{\partial \chi_-} \quad \text{where } \frac{\mathrm{d}\chi_-}{\mathrm{d}\tau} = V - 1 - \frac{3}{4}R - \frac{1}{4}\alpha. \tag{3.41}$$

The corresponding water depth and surface elevation are determined by

$$d = \left(1 + \tfrac{1}{4}(R-\alpha)\right)^2 \quad \text{and} \quad \eta = d - 1 + \Gamma. \tag{3.42}$$

It is straightforward to solve (3.41) numerically by tracking the $\chi_-(\tau)$ characteristics from their origin, and phenomena associated with subcritical, supercritical and transcritical flow conditions can easily be handled, in contrast to the original two-family system (3.5)–(3.7).

3.3.2. *The Hopf formulation*

The Hopf equation solved by Grimshaw & Smyth (1986) can be retrieved from (3.41), by once again assuming that $\Gamma = O(\varepsilon^2)$, i.e. one order of magnitude smaller than the surface elevation, and two orders smaller than the water depth. By utilizing (3.29), (3.13), (3.35) and (3.40) we find that

$$c \simeq 1 + \varepsilon\frac{\eta}{2} + O(\varepsilon^2), \quad \alpha = O(\varepsilon^2), \quad R \simeq 2\eta + O(\varepsilon^2), \tag{3.43}$$

by which (3.41) simplifies to

$$\frac{\mathrm{D}\eta}{\mathrm{D}\tau} = \frac{1}{2}\frac{\partial \Gamma}{\partial \chi_-} \quad \text{where } \frac{\mathrm{d}\chi_-}{\mathrm{d}\tau} = V - 1 - \frac{3}{2}\eta. \tag{3.44}$$

This is the Hopf equation imbedded in the forced KdV equation.

3.3.3. *A comparison between the AMOC, Hopf and NSW formulations*

In order to make a preliminary comparison with the original NSW equations as given in (3.5)–(3.7), we have considered an obstacle defined by (2.4) with $\Gamma_m = 0.10$ and $L = 100$. Figure 2(*a*) shows the subcritical case of $V = 0.45$ at time $\tau = 300$, while figure 2(*b*) shows the supercritical case of $V = 1.60$ at time $\tau = 200$. In both cases the numerical AMOC solution (dashed line) is in remarkably good agreement with the NSW solution (the full grey line). In fact you can hardly tell the difference between the two curves, except in the far downstream region ($\chi \simeq 400$ in figure 2*a* and $\chi \simeq 500$ in figure 2*b*). The bound solutions over the obstacle ($-50 < \chi < 50$) as well as the forward-going free waves (appearing at $\chi \simeq -190$ in figure 2*a*, and at $\chi \simeq 150$ in figure 2*b*) are almost identical. However, in fact it is even more remarkable that the single-family AMOC solution is able to capture the backward-going free waves (appearing for $\chi \simeq 450$–$550$). This is possible due to the memory

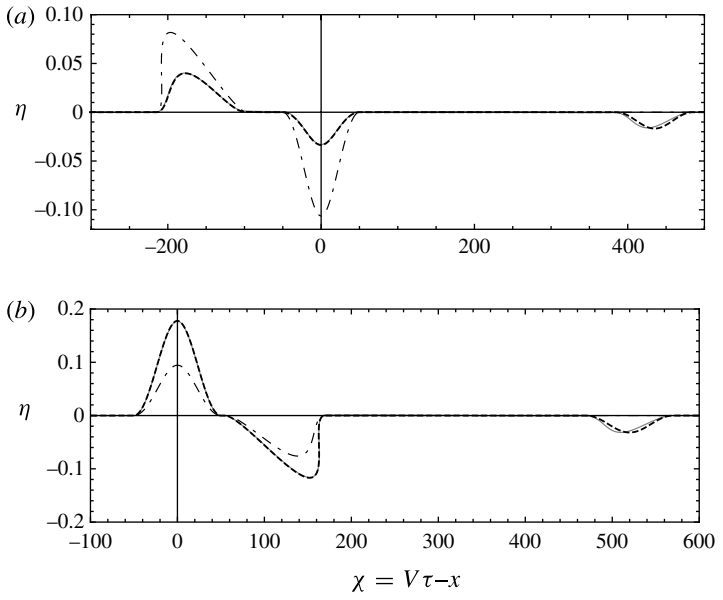


FIGURE 2. Snapshots of the computed surface elevation for (*a*) a subcritical case with $V = 0.45$ and $\tau = 300$ and (*b*) a supercritical case with $V = 1.60$ and $\tau = 200$, and for $\Gamma_m = 0.10$, $L = 100$. Full grey line: two-family MOC solution to the NSW equations defined by (3.5)–(3.7); dashed line: single-family AMOC solution to (3.41); dashed-dotted line: solution to the Hopf (fKdV) equation defined by (3.44).

effect incorporated in $\alpha$ given by (3.35). The accuracy of the backward-going free wave is not perfect, but still good enough to secure a high accuracy of the forward-going free wave. In contrast, the numerical Hopf solutions (dot-dashed line) are completely off: for the subcritical/supercritical case the bound solution as well as the forward-going free waves are significantly overestimated/underestimated, while the backward-going free wave is not captured at all. However, it should be emphasized that this test is really violating the restrictions for the Hopf solution: as discussed in the introduction, the forced KdV equation requires that $V - 1 = O(\varepsilon)$, which implies that the Hopf equation is really not applicable for subcritical and supercritical conditions.

## 4. Analytical solutions to the new AMOC formulation of the NSW equations

Grimshaw & Smyth (1986) derived an exact analytical solution to (3.44) by integrating it along the $\chi_-(\tau)$ characteristics. Their analytical solution provided a very informative perception of the flow details and phenomena to be observed in transcritical flow, and it could be used to determine not only the asymptotic solution but also temporal and spatial details, which matched numerical solutions to (3.44). In the following, we shall pursue the possibility of deriving a similar analytical solution to the new AMOC formulation (3.41), which will cover not only transcritical flow but also subcritical and supercritical flow. It turns out that we can only achieve an approximative solution to (3.41), which nevertheless is convenient, informative and fairly accurate.

### 4.1. *Analytical integration of the $\chi_-(\tau)$ characteristics*

The first step towards an analytical solution to (3.41), is to multiply the characteristic equation by the characteristic speed, by which the right-hand side becomes

$$\frac{\mathrm{d}\chi_-}{\mathrm{d}\tau}\frac{\partial \Gamma}{\partial \chi_-} = \frac{\mathrm{D}\Gamma}{\mathrm{D}\tau}, \tag{4.1}$$

while the left-hand side becomes

$$\frac{\mathrm{d}\chi_-}{\mathrm{d}\tau}\frac{\mathrm{D}R}{\mathrm{D}\tau} = \left(V - 1 - \frac{3}{4}R - \frac{1}{4}\alpha\right)\frac{\mathrm{D}R}{\mathrm{D}\tau}. \tag{4.2}$$

The first three terms on the right-hand side of (4.2) can easily be written in conservation form, while the last term calls for an additional approximation: we assume that $\alpha$, which basically is a function of $\Gamma$, varies more slowly with $\chi_-(\tau)$ than $R$, and use the approximation

$$-\frac{1}{4}\alpha\frac{\mathrm{D}R}{\mathrm{D}\tau} \simeq \frac{\mathrm{D}}{\mathrm{D}\tau}\left(-\frac{1}{4}\alpha R\right). \tag{4.3}$$

This leads to the following approximative conservation form of (3.41):

$$\frac{\mathrm{D}}{\mathrm{D}\tau}\left(\frac{3}{8}R^2 - \left(V - 1 - \frac{1}{4}\alpha\right)R + \Gamma\right) = 0. \tag{4.4}$$

Next, we integrate (4.4) along $\chi_-(\tau)$ starting from $\chi_-(0)$, and in this connection the integration constant becomes

$$G_0[\chi_-(0)] \equiv \tfrac{3}{8}R_0^2 - (V - 1 - \tfrac{1}{4}\alpha_0)R_0 + \Gamma[\chi_-(0)], \tag{4.5}$$

where $\alpha_0$ is given by (3.36), and where

$$R_0 \equiv R[\chi_-(0)] = 2\left(\sqrt{1 - \Gamma[\chi_-(0)]} - 1\right). \tag{4.6}$$

We note that $G_0$ goes to zero for $|\chi_-(0)| \geqslant L/2$, while it reaches its maximum $G_{0m}$ for $\chi_-(0) = 0$, i.e.

$$G_{0m} = \tfrac{3}{8}R_{0m}^2 - (V - 1 - \tfrac{1}{4}\alpha_{0m})R_{0m} + \Gamma_m, \tag{4.7}$$

$$R_{0m} = 2\left(\sqrt{1 - \Gamma_m} - 1\right), \quad \alpha_{0m} = 2 - 2\sqrt{1 - \Gamma_m}. \tag{4.8}$$

By integrating (4.4), using (4.5), and solving with respect to $R$, we finally obtain

$$R = \tfrac{4}{3}\left(\beta \mp \sqrt{\beta^2 + \tfrac{3}{2}(G_0 - \Gamma)}\right) \quad \text{where } \beta \equiv V - 1 - \tfrac{1}{4}\alpha. \tag{4.9}$$

In the following we shall discuss this solution in connection with transcritical flow, subcritical flow and supercritical flow.

### 4.2. *The essential characteristics and the classification of flow regimes*

#### 4.2.1. *The concept of turning points and the limiting characteristic*

The concept of turning points is a unique feature of transcritical flow. A turning point occurs whenever the characteristic speed goes to zero, and according to (3.41) this happens for

$$R \to \tfrac{4}{3}(V - 1 - \tfrac{1}{4}\alpha). \tag{4.10}$$

This, on the other hand, coincides with the situation where the square-root terms in (4.9) cancel, i.e.

$$(V - 1 - \tfrac{1}{4}\alpha)^2 + \tfrac{3}{2}(G_0 - \Gamma) \to 0. \tag{4.11}$$

Now, let us consider the limiting characteristic (*lc*), which starts from $\chi_-(0) = \chi_0^{lc}$ and reaches its turning point precisely at $\chi_-(\tau) = 0$, i.e. at the crest of the obstacle. This particular characteristic will asymptotically stop and remain at $\chi = 0$, and therefore it will eventually govern the bound solution at the crest of the obstacle. Characteristics starting closer to the crest of the obstacle will experience no turning but continue over the obstacle, while the characteristics starting further away from the crest will turn before reaching the crest and return to where they came from. For this reason, it is the limiting characteristic and its immediate neighbours (starting from $\chi_0^{lc} \pm \delta$ where $\delta \to 0$), which govern the asymptotic bound solution in the vicinity of the obstacle. Now let $\alpha$ be approximated by its asymptotic expression (3.37), and require that (4.11) goes to zero for $\Gamma = \Gamma_m$. This leads to the condition

$$G_0^{lc} = \Gamma_m - \frac{2}{3}\left(V - 1 - \frac{1}{4}\frac{\Gamma_m}{V+1}\right)^2. \tag{4.12}$$

Provided that $G_0^{lc}$ obtained from (4.12) satisfies $0 \leqslant G_0^{lc} \leqslant G_{0m}$, we can now determine the corresponding value of $\chi_0^{lc}$ by combining (4.12) and (4.5). Examples are given in figure 4, which is discussed in § 4.2.5.

4.2.2. *Classification of flow regimes*

The special case of $G_0^{lc} = 0$ defines the transition from transcritical flow to subcritical or supercritical flow. The subcritical transition occurs for $\chi_0^{lc} \to L/2$ and $V = V_{low} < 1$, while the supercritical transition occurs for $\chi_0^{lc} \to -L/2$ and $V = V_{high} > 1$. Combining the condition $G_0^{lc} = 0$ with (4.12) yields the implicit AMOC expression

$$\Gamma_m = \frac{2}{3}\left(V - 1 - \frac{1}{4}\frac{\Gamma_m}{V+1}\right)^2, \tag{4.13}$$

which defines the limits $V_{low}$ and $V_{high}$ as a function of $\Gamma_m$. We emphasize that, due to the approximations involved in the analytical integration of the AMOC formulation, (4.13) differs from the corresponding expression derived directly from the steady NSW equations, e.g.

$$\Gamma_m = 1 + \tfrac{1}{2}V^2 - \tfrac{3}{2}V^{2/3}. \tag{4.14}$$

Note also that the corresponding expression for the Hopf equation reads

$$\Gamma_m = \tfrac{2}{3}(V - 1)^2, \tag{4.15}$$

which leads to the explicit solutions

$$V_{low} = 1 - \sqrt{\tfrac{3}{2}\Gamma_m} \quad \text{and} \quad V_{high} = 1 + \sqrt{\tfrac{3}{2}\Gamma_m}. \tag{4.16}$$

Figure 3 shows that (4.16) is surprisingly accurate, especially considering that the Hopf equation formally requires that $V - 1 = O(\varepsilon)$ and $\Gamma_m = O(\varepsilon^2)$. On this basis we recommend classifying the flow conditions over the obstacle by the following

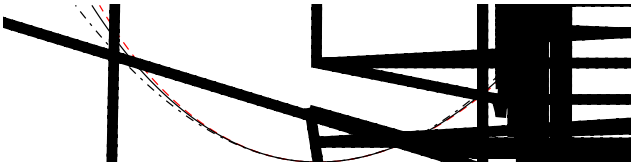

FIGURE 3. (Colour online) Basic thresholds between subcritical, lower-transcritical, higher-transcritical and supercritical flow. Full line: NSW solution to (4.14); dot-dashed line: Hopf solution (4.15); dashed line: AMOC solution to (4.13); dotted line: AMOC solution to (4.18).

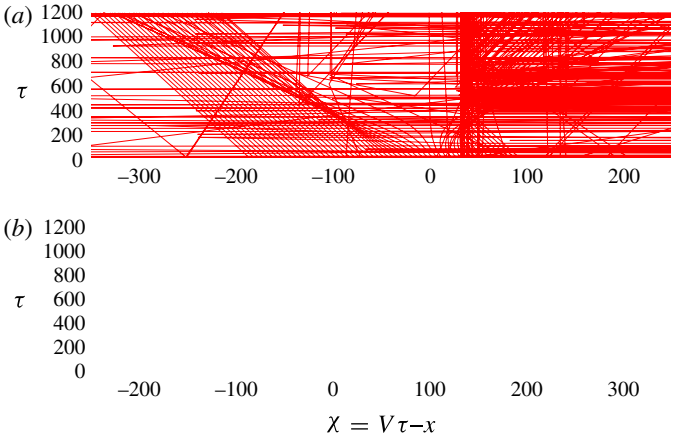


FIGURE 4. (Colour online) The characteristic tracks $\chi_-(\tau)$ determined from (3.41) for $\Gamma_m = 0.05$, $L = 100$. (*a*) Lower-transcritical case: $\Phi = -0.5$; (*b*) higher-transcritical case: $\Phi = 0.5$.

parameter:

$$\Phi \equiv \sqrt{\frac{2}{3}}\frac{\Delta}{\sqrt{\Gamma_m}}, \quad \text{where } \Delta \equiv V - 1. \tag{4.17}$$

Hence we introduce the limits $\Phi_{low}$ and $\Phi_{high}$ based on (4.17) with $V_{low}$ and $V_{high}$, respectively. Note that (4.17) has the advantage that it combines the effect of the height and the speed of the obstacle, and for the case of the Hopf solution we obtain the approximate flow limits of $\Phi_{low} = -1$ and $\Phi_{high} = 1$. We shall utilize the definition (4.17) throughout the rest of this paper.

4.2.3. *The crest characteristic starting from the crest of the obstacle*

Another unique characteristic is the one starting at the location of the crest of the obstacle, i.e. at $\chi_-(0) = 0$. For subcritical flow, i.e. $V < V_{low}$, this crest characteristic governs the magnitude of the forward-going free wave, which propagates in the upstream region ahead of the obstacle. Similarly, for supercritical flow, i.e. $V_{high} < V$, it governs the magnitude of the forward-going free wave, which now occurs in the downstream region behind the obstacle.

Remarkably, the crest characteristic also plays an important role in transcritical flow, despite the presence of turning points. In this connection, it turns out to be convenient

to introduce the concepts of lower-transcritical and higher-transcritical flow conditions defined as $V_{low} < V < V_{mid}$ and $V_{mid} < V < V_{high}$, respectively. The threshold $V_{mid}$ satisfies the condition

$$G_0^{lc} = G_{0m} \Rightarrow V = V_{mid}, \tag{4.18}$$

and the determination of $V_{mid}$ involves a combination of (4.18), (4.12) and (4.7). The Hopf equation leads to $V_{mid} = 1$, while the AMOC solution generally leads to slightly lower values. Note that for $V = V_{mid}$, we obtain $\chi_0^{lc} = 0$, and this implies that the turning points in the transcritical solution vanish. Consequently the characteristics starting from $\chi_-(0) < 0$ will radiate upstream, while the ones with $\chi_-(0) > 0$ will radiate downstream.

For lower-transcritical flow conditions, the crest characteristic will govern the magnitude of the leading forward-going free wave, which propagates in the upstream region ahead of the obstacle. This situation is very similar to what happens in subcritical flow. For higher-transcritical flow conditions, the crest characteristic will influence the leading forward-going free wave, which now propagates in the

All the characteristics starting from $\chi_-(0) \leqslant -L/2$ will turn exactly at the caustic $\chi_b = -33.52$. Finally, it should be emphasized that we generally allow the characteristics to cross and produce double-valued solutions even though this situation heralds the onset of shock waves.

### 4.3. *Asymptotic expressions for transcritical flow*

#### 4.3.1. *The AMOC solution*

We consider the transcritical regime defined by $\Phi_{low} < \Phi < \Phi_{high}$, and assume that shock waves do not occur in the region $-L/2 \leqslant \chi \leqslant L/2$ over the obstacle. Similar assumptions were made by Grimshaw & Smyth (1986) and El *et al.* (2009), but we emphasize that these assumptions are sometimes violated (examples will be given later).

As discussed in § 4.2.1, the asymptotic bound solution in the vicinity of the obstacle is governed by the limiting characteristic coming from $\chi_-(0) = \chi_0^{lc}$. Hence at the upstream and downstream toes of the moving obstacle we use (4.9) with $G_0 = G_0^{lc}$ and $\chi_-(\tau) = \pm L/2$, which implies that $\alpha$ and $\Gamma$ go to zero. This leads to

$$R_{bound}^{up} = \tfrac{4}{3}\left(\Delta + \sqrt{\Delta^2 + \tfrac{3}{2}G_0^{lc}}\right), \quad R_{bound}^{down} = \tfrac{4}{3}\left(\Delta - \sqrt{\Delta^2 + \tfrac{3}{2}G_0^{lc}}\right). \tag{4.20}$$

More generally, we may express the $\chi$ variation of the asymptotic bound solution for $R$ as

$$R_{bound}(\chi) = \tfrac{4}{3}\left(\beta_1(\chi) + \kappa\sqrt{\beta_1(\chi)^2 + \tfrac{3}{2}\left(G_0^{lc} - \Gamma(\chi)\right)}\right) \quad \text{for} \quad -\frac{L}{2} \leqslant \chi \leqslant -\frac{L}{2}, \tag{4.21}$$

where

$$\beta_1(\chi) \equiv \Delta - \frac{1}{4}\frac{\Gamma(\chi)}{V+1}, \quad \kappa \equiv -\mathrm{sign}(\chi). \tag{4.22}$$

Note that at $\chi = 0$, the general expression (4.21)–(4.22) can be simplified by using (4.12), which leads to

$$R_{bound}^{crest} = \frac{4}{3}\left(\Delta - \frac{1}{4}\frac{\Gamma_m}{V+1}\right). \tag{4.23}$$

As discussed in § 4.2.3, the asymptotic free solution is governed by the crest characteristic starting from $\chi_-(0) = 0$. In this case we use (4.9) with $G_0 = G_{0m}$, $\alpha = 0$ and $\Gamma = 0$, which leads to

$$R_{free}^{up} = \tfrac{4}{3}\left(\Delta + \sqrt{\Delta^2 + \tfrac{3}{2}G_{0m}}\right) \quad \text{for } \Phi_{low} < \Phi \leqslant \Phi_{mid}, \tag{4.24}$$

$$R_{free}^{down} = \tfrac{4}{3}\left(\Delta - \sqrt{\Delta^2 + \tfrac{3}{2}G_{0m}}\right) \quad \text{for } \Phi_{mid} \leqslant \Phi < \Phi_{high}. \tag{4.25}$$

We note that for $\Phi = \Phi_{mid}$, (4.24)–(4.25) match the bound solutions (4.20), i.e. $R_{free}^{up} = R_{bound}^{up}$ and $R_{free}^{down} = R_{bound}^{down}$. It is emphasized that the corresponding solutions for $\eta$ are determined by utilizing (3.42).

#### 4.3.2. *The Hopf solution*

For comparison, let us again assume that $\Gamma = O(\varepsilon^2)$, i.e. one order of magnitude smaller than the surface elevation. In this case (4.6) simplifies to $R_0 = 0$, while (4.5)

and (4.12) simplify to

$$G_0[\chi_-(0)] = \Gamma[\chi_-(0)] \quad \text{and} \quad G_0^{lc} = \Gamma_m - \tfrac{2}{3}\Delta^2. \tag{4.26}$$

Now the asymptotic bound solution (4.21) simplifies to

$$\eta_{bound}(\chi) = \tfrac{2}{3}\left(\Delta + \kappa\sqrt{\Delta^2 + \tfrac{3}{2}(G_0^{lc} - \Gamma(\chi))}\right) \quad \text{where } \kappa \equiv -\text{sign}(\chi), \tag{4.27}$$

which leads to

$$\eta_{bound}^{up} = \tfrac{2}{3}\left(\Delta + \sqrt{\tfrac{3}{2}\Gamma_m}\right), \quad \eta_{bound}^{crest} = \tfrac{2}{3}\Delta, \quad \eta_{bound}^{down} = \tfrac{2}{3}\left(\Delta - \sqrt{\tfrac{3}{2}\Gamma_m}\right). \tag{4.28}$$

### 4.4. *Asymptotic expressions for subcritical and supercritical flow*

For subcritical and supercritical conditions, the asymptotic bound solution surrounding the moving obstacle is determined by characteristics coming from infinity, i.e. $G_0 = 0$. In this case (4.9) leads to

$$R_{bound}(\chi) = \tfrac{4}{3}\left(\beta_1(\chi) + \kappa\sqrt{\beta_1(\chi)^2 - \tfrac{3}{2}\Gamma(\chi)}\right) \quad \text{for } -\frac{L}{2} \leqslant \chi \leqslant -\frac{L}{2}, \tag{4.29}$$

where $\beta_1$ is defined by (4.22), and where $\kappa = 1$ for $\Phi < \Phi_{low}$ and $\kappa = -1$ for $\Phi > \Phi_{high}$. The corresponding solution to the Hopf equation reads

$$\eta_{bound}(\chi) = \tfrac{2}{3}\left(\Delta + \kappa\sqrt{\Delta^2 - \tfrac{3}{2}\Gamma(\chi)}\right), \tag{4.30}$$

where $\kappa = 1$ for $\Phi < -1$ and $\kappa = -1$ for $\Phi > 1$.

Finally, the forward-going free wave is governed by the crest characteristic starting from $\chi_-(0) = 0$, and by using (4.9) with $G_0 = G_{0m}$, $\alpha = 0$ and $\Gamma = 0$ we obtain

$$R_{free}^{up} = \tfrac{4}{3}\left(\Delta + \sqrt{\Delta^2 + \tfrac{3}{2}G_{0m}}\right) \quad \text{for } \Phi \leqslant \Phi_{low}, \tag{4.31}$$

$$R_{free}^{down} = \tfrac{4}{3}\left(\Delta - \sqrt{\Delta^2 + \tfrac{3}{2}G_{0m}}\right) \quad \text{for } \Phi_{high} \leqslant \Phi. \tag{4.32}$$

Notice that (4.31)–(4.32) match and continue the expressions (4.24)–(4.25) valid in the transcritical regime. It is emphasized that the corresponding solutions for $\eta$ are determined by utilizing (3.42).

## 5. The formation of shock waves and undular bores

Whenever the NSW characteristics of the same family cross, the solution starts to produce overturning waves, and this heralds the formation of a shock wave (see e.g. Stoker 1958, his § 10.10 with figures 10.10.8 and 10.10.9). The shock wave (at least in a mathematical sense) moves with a vertical front face, i.e. as a discontinuity in the surface elevation, and for weak shocks its celerity can be approximated as the average speed of the two crossing characteristics. For stronger shocks the general expressions given in § 2 should be applied.

For the relatively low obstacles considered in this work, the discontinuity should be replaced by a dispersive undular bore, which cannot be captured by the NSW equations. Instead we need KdV or Boussinesq equations including a mixture of nonlinearity and dispersion. Gurevich & Pitaevskii (1974) were the first to provide a

mathematical description of an undular bore generated by an initial discontinuity in the surface elevation. They used the modulation theory by Whitham (1974) in connection with the KdV equation, and showed that the bore can be described as a modulated train of cnoidal waves with a leading solitary wave in front and small sinusoidal waves trailing behind. They derived asymptotic expressions for the temporal and spatial variations of the surface elevation including the propagation speed of the leading and trailing edges of the bore. Later, Grimshaw & Smyth (1986) and Smyth (1987) extended this description to cover upstream and downstream bores in connection with transcritical flow over a bottom obstacle. A comprehensive and systematic review of these methods has been given by Kamchatnov (2000).

Recently, El, Grimshaw & Smyth (2006) and El *et al.* (2009) developed a far-field modulation solution for undular bores in the framework of the Boussinesq equations by Su & Gardner (1969). They were not able to describe the actual evolution of the surface elevation, but provided expressions for the height and speed of the leading and trailing edges of the upstream and downstream undular bores. The non-dispersive near-field solution over the obstacle was covered by a slightly modified version of Houghton & Kasahara's (1968) asymptotic formulation for bound waves.

In the following we shall concentrate on the propagation speeds of the leading and trailing edges of the bores in the framework of the NSW and KdV formulations.

### 5.1. *Leading downstream edge*

The leading edge of the downstream bore is assumed to travel over a flat bottom as a solitary wave of height $H_D$, in a depth $d_D = 1 + \eta_D$, and in an ambient current $U_D$. In a fixed frame of reference the celerity can be expressed as

$$c^-_{down} = U_D + \sqrt{d_D + H_D}, \tag{5.1}$$

where the velocity $U_D$ is determined by (3.34) with $\alpha = 0$. The remaining problem is therefore to estimate the wave height $H_D$. In the framework of the KdV equation, Gurevich & Pitaevskii (1974) and Grimshaw & Smyth (1986) established the result $H_D = -2\eta_D > 0$, and in combination with (5.1) and (3.34) this leads to

$$c^-_{down} = 2\left(\sqrt{1+\eta_D} - 1\right) + \sqrt{1-\eta_D}. \tag{5.2}$$

Note that for small values of $\eta_D$, (5.2) simplifies to $c^-_{down} \simeq 1 + \eta_D/2$, and by inserting the Hopf expression (4.28) we obtain

$$c^-_{down} \simeq 1 + \tfrac{1}{3}\Delta - \sqrt{\tfrac{1}{6}\Gamma_m}, \tag{5.3}$$

which is the fKdV result obtained by Grimshaw & Smyth (1986).

A more sophisticated estimate of $H_D$ was recently derived by El *et al.* (2009) on the basis of the Boussinesq equations by Su & Gardner (1969). Their result can be expressed as

$$H_D = (1+\eta_D)\left(\lambda^2 - 1\right) \quad \text{and} \quad c^-_{down} = 2\left(\sqrt{1+\eta_D} - 1\right) + \lambda\sqrt{1+\eta_D}, \tag{5.4}$$

where $\lambda$ satisfies

$$(1+\eta_D)\sqrt{\lambda} - \left(\frac{4-\lambda}{3}\right)^{21/10}\left(\frac{1+\lambda}{2}\right)^{2/5} = 0. \tag{5.5}$$

In practice there is little difference between (5.4) and (5.2) up to the point where $\eta_D$ exceeds 35–40 % of the still water depth.

FIGURE 5. (Colour online) The attachment of upstream and downstream bores as a function of $\Gamma_m$. Dashed line: the KdV solution for attachment.

The downstream bore becomes attached to the obstacle whenever $c^-_{down} \to V$, and we denote this incidence as $\Phi_a^{down}$. This criterion is shown in figure 5 as a function of $\Gamma_m$. For comparison the corresponding KdV solution based on (5.3) leads to $\Phi_a^{down} = -0.5$. The downstream bore will be attached to the obstacle in the interval $\Phi_{low} < \Phi \leqslant \Phi_a^{down}$.

### 5.2. *Leading upstream edge*

The leading edge of the upstream bore is assumed to travel over a flat bottom as a solitary wave of height $H_B$, in a depth $d_A = 1$, and in the ambient current $U_A = 0$. In a fixed frame of reference the celerity can be expressed as

$$c^-_{up} = \sqrt{1 + H_B}. \tag{5.6}$$

Again we need to estimate the wave height $H_B$. By using the findings of Gurevich & Pitaevskii (1974) and Grimshaw & Smyth (1987), we get $H_B = 2\eta_B > 0$, which leads to

$$c^-_{up} = \sqrt{1 + 2\eta_B}. \tag{5.7}$$

Note that for small values of $\eta_B$, (5.7) simplifies to $c^-_{up} \simeq 1 + \eta_B$, and by inserting the Hopf expression (4.28) we obtain

$$c^-_{up} \simeq 1 + \tfrac{2}{3}\Delta + \sqrt{\tfrac{2}{3}\Gamma_m}, \tag{5.8}$$

which is the KdV result obtained by Grimshaw & Smyth (1986).

A more sophisticated estimate of $H_D$ was derived by El *et al.* (2009) on the basis of the Boussinesq equations by Su & Gardner (1969). In this case their result can be expressed as

$$H_B = \left(\lambda^2 - 1\right) \quad \text{and} \quad c^-_{up} = \lambda, \tag{5.9}$$

where $\lambda$ satisfies

$$\frac{\sqrt{\lambda}}{1 + \eta_B} - \left(\frac{4 - \lambda}{3}\right)^{21/10} \left(\frac{1 + \lambda}{2}\right)^{2/5} = 0. \tag{5.10}$$

Again, there is little difference between (5.9) and (5.7) up to the point where $\eta_B$ exceeds 35–40 % of the still water depth.

However, it should be emphasized that El *et al.* (2009) generally combined (5.9)–(5.10) with the choice of $\eta_B = \eta_{bound}^{up}$. As discussed throughout § 4, a better choice would be $\eta_B = \eta_{free}^{up}$ determined from (4.24) if $\Phi_{low} < \Phi < \Phi_{mid}$, and $\eta_B = \eta_{bound}^{up}$ determined from (4.20) if $\Phi_{mid} < \Phi < \Phi_{high}$.

### 5.3. *Trailing upstream edge*

As long as the undular bore is completely detached from the moving body and moves over a constant depth, the trailing edge of the bore will move with the group velocity of the cnoidal wave train. Within the framework of KdV theory and measured in the fixed frame of reference, the group velocity reads

$$c_{up}^{+} = 1 - \Delta - \sqrt{\tfrac{3}{2}\Gamma_m}. \tag{5.11}$$

El *et al.* (2009) extended this expression to

$$c_{up}^{+} = 2\left(\sqrt{1+\eta_B} - 1\right) + \lambda^3\sqrt{1+\eta_B}, \tag{5.12}$$

where the first term accounts for the ambient-current velocity, the second term for the group velocity, and where $\lambda$ satisfies

$$(1+\eta_B)\sqrt{\lambda} - \left(\frac{4-\lambda}{3}\right)^{21/10}\left(\frac{1+\lambda}{2}\right)^{2/5} = 0. \tag{5.13}$$

In this case $\eta_B = \eta_{bound}^{up}$ is always the relevant level to apply in connection with (5.12)–(5.13).

The upstream bore becomes attached to the obstacle whenever $c_{up}^{+} \to V$, and we denote this incidence as $\Phi_a^{up}$. This criterion is shown in figure 5 as a function of $\Gamma_m$. For comparison the corresponding KdV solution based on (5.11) leads to $\Phi_a^{up} = -0.5$. The upstream bore will be attached to the obstacle in the interval $\Phi_a^{up} \leqslant \Phi \leqslant \Phi_{high}$.

## 6. Numerical results and comparisons

In this section, we demonstrate that the numerical solution to the new single-family formulation of the NSW equations can predict the initial temporal and spatial evolution of the transient waves associated with the moving bottom obstacle. Typically, the solution will approach a bound steady state over most parts of the obstacle, which is also valid asymptotically, and this implies that dispersion can generally be ignored within this region. At some distance from the obstacle, dispersion will become important sooner or later, and beyond this point a Boussinesq formulation will be much more appropriate for the detailed modelling of the upstream and downstream waves. But even beyond this point, the non-dispersive asymptotic predictions obtained by the new theory are useful, e.g. for estimating the expected height and speed of the leading upstream waves, the upstream/downstream setup/setdown at the toe of the obstacle, and the height and speed of the leading downstream waves. This also allows a prediction of when the upstream and downstream bores become attached to or detached from the obstacle.

Our main vehicle for establishing reference solutions for the transient wave problem is a numerical model, which solves the high-order Boussinesq formulation by Madsen, Fuhrman & Wang (2006), see also Madsen *et al.* (2002, 2003). This method uses exact representations of the kinematic and dynamic free-surface conditions expressed in terms of surface velocities, and determines the vertical distribution of fluid

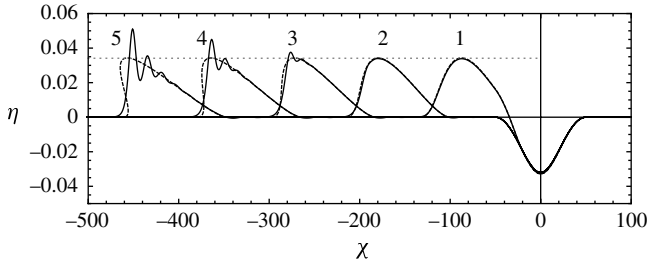


FIGURE 6. Snapshots (at five different times) of the surface elevation for subcritical conditions: $\Phi = -1.5$, $\Gamma_m = 0.05$ and $L = 100$. Comparison between the AMOC simulation (dashed line) and a Boussinesq simulation (full line). Dotted line: the asymptotic level $\eta^{up}_{free}$ based on (4.31). Snapshots shown at (1) $\tau = 200$; (2) $\tau = 400$; (3) $\tau = 600$; (4) $\tau = 800$; (5) $\tau = 1000$.

velocity through a Padé-enhanced truncated series solution to the Laplace equation. As demonstrated in many previous studies, this formulation can accurately treat nonlinear dispersive waves even for a wavenumber times the water depth as high as 30. This is more than sufficient for the present problem, which is basically a shallow water problem with relatively weak dispersion. Fuhrman & Madsen (2009) recently extended the model to allow for a time-varying bottom and a moving shoreline in connection with tsunami generation. The numerical solution procedure is based on finite-difference discretizations on an equidistant grid, and an explicit four-stage fourth-order Runge–Kutta scheme is used for the time integration. A detailed description of the scheme can be found in Madsen *et al.* (2002) for one horizontal dimension. The examples presented in this section have been simulated using the following non-dimensional discretization: $\mathrm{d}x = 0.25$–$0.5$ and $\mathrm{d}\tau = 0.1$–$0.2$ keeping the Courant number at $Cr = \mathrm{d}\tau/\mathrm{d}x = 0.4$. For most cases, this choice is adequate for describing the waves appearing in the upstream and downstream bores; however it should be mentioned that near the transitions $\Phi_{low}$ and $\Phi_{high}$ the leading waves become very high and steep and somewhat under-resolved.

### 6.1. *Verification of the temporal and spatial evolution of the surface elevation*

In this first investigation covering figures 6–12, we have considered the moderate obstacle height of $\Gamma_m = 0.05$. This leads to the following set of governing parameters: firstly, the thresholds for transcritical flow (see § 4.2.2) are $\Phi_{low} = -0.974$ and $\Phi_{high} = 1.020$; secondly, the transition from lower- to higher-transcritical flow (see § 4.2.3) occurs at $\Phi_{mid} = -0.035$; thirdly, the upstream and downstream attachment thresholds (see §§ 5.1 and 5.3) are $\Phi^{up}_a = -0.452$ and $\Phi^{down}_a = -0.595$ (see also figure 5).

Figure 6 covers the subcritical case of $\Phi = -1.5$ (with $L = 100$). The computed spatial variation of the surface elevation (shown for $\tau = 200$, 400, 600, 800 and 1000) includes the forward-going free wave as well as the bound wave (appearing at $-50 < \chi < 50$), while the backward-going free wave has been left out of the picture. For the first two instants there is hardly any difference between the AMOC solution (dashed line) and the Boussinesq solution (full line). Then at $\tau = 600$ dispersion starts to play a minor role at the crest of the forward-going free wave, and this trend further evolves at $\tau = 800$ and $\tau = 1000$, where the AMOC solution starts to produce overturning waves. The crest of the AMOC solution for the forward-going free wave

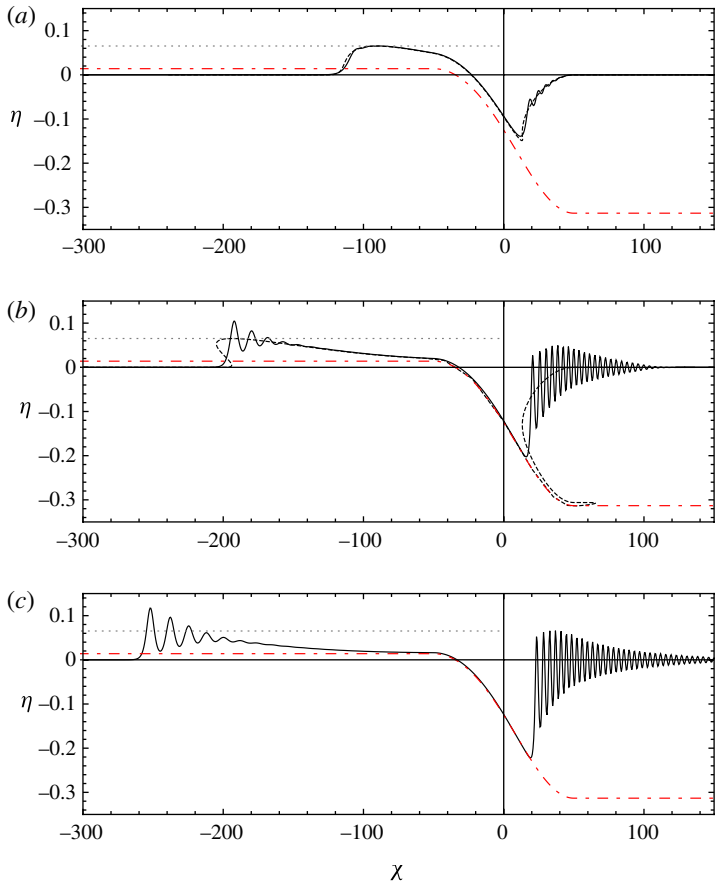


FIGURE 7. (Colour online) Snapshots, at times (*a*) $\tau = 300$, (*b*) $\tau = 600$ and (*c*) $\tau = 800$, of the surface elevation for lower-transcritical conditions: $\Phi = -0.9$, $\Gamma_m = 0.05$ and $L = 100$. Comparison between the AMOC simulation (dashed line) and a Boussinesq simulation (full line). Dashed-dotted curve: the asymptotic level $\eta_{bound}$ based on (4.21); dotted line: the asymptotic level $\eta^{up}_{free}$ based on (4.24).

clearly follows the analytical AMOC estimate $\eta^{up}_{free}$ based on (4.31), which is shown as the horizontal dotted line. The bound wave over the obstacle does not change beyond $\tau = 400$, and there is an excellent agreement between the AMOC solution and the Boussinesq solution.

Figure 7 covers the lower-transcritical case of $\Phi = -0.9$ (with $L = 100$). Since $\Phi < \Phi_{mid} = -0.035$, we expect the leading edge of the upstream bore to follow $\eta^{up}_{free}$, while the trailing edge should follow $\eta^{up}_{bound}$ (see the discussion in §§ 4.2.1 and 4.2.3). Furthermore, since $\Phi_{low} < \Phi < \Phi^{down}_{a}$, we expect the downstream bore to become attached to the obstacle. The computed spatial variation of the surface elevation is shown in figure 7(*a–c*) for $\tau = 300$, 600 and 800, respectively. The figures also include a horizontal dotted line representing $\eta^{up}_{free}$ based on (4.24), and a dash-dotted curve representing $\eta_{bound}(\chi)$ based on (4.21).

At $\tau = 300$ the numerical AMOC solution (dashed line) agrees very well with the Boussinesq solution (full line) except for the weak signs of dispersion seen in the

downstream transition to still water. At this stage, both solutions deviate significantly from the asymptotic $\eta_{bound}$, while the crest of the upstream-going wave follows $\eta_{free}^{up}$ very closely. At $\tau = 600$ the AMOC solution matches the Boussinesq solution quite closely in the upstream region ($\chi < 0$), except for the very front of the bore, where dispersion starts to play a role. In the front of the upstream bore, the AMOC solution still follows $\eta_{free}^{up}$, while the Boussinesq solution tends to grow somewhat higher due to the formation of shorter and higher cnoidal waves. At this stage, the AMOC solution and the Boussinesq solution agree very well with the asymptotic $\eta_{bound}$ over part of the obstacle ($-50 \leqslant \chi < 20$). However, at the downstream location $\chi \simeq 20$, an undular bore develops in the Boussinesq solution, and this obviously violates the non-dispersive assumptions for $\eta_{bound}$. No attempts have been made to capture the formation of shock waves in the AMOC formulation, but from its strongly overturning pattern we can see that shock waves would indeed occur over the obstacle. This is clearly a situation which violates the basis for the AMOC solution as well as for the NSW equations in the downstream region. Finally, at $\tau = 800$ we have omitted the numerical AMOC solution, because it no longer makes sense. Again we notice that the Boussinesq solution agrees well with $\eta_{bound}$ in the region $-50 < \chi < 20$, while it is clear that the downstream undular bore is attached to the obstacle (as predicted) at approximately $\chi = 20$.

Figure 8 shows the lower-transcritical case of $\Phi = -0.5$ (with $L = 100$). Since $\Phi < \Phi_{mid}$, the leading edge of the upstream bore is again expected to follow $\eta_{free}^{up}$, while the trailing edge should follow $\eta_{bound}^{up}$. Furthermore, since $\Phi_a^{down} < \Phi < \Phi_a^{up}$, we expect the downstream and upstream bores to be detached from the obstacle. The computed spatial variation of surface elevation is shown in figure 8(*a–c*) for $\tau = 100$, 300 and 1000, respectively. At $\tau = 100$ the AMOC solution and the Boussinesq solution are almost identical even with respect to the small backward-going free wave located at $\chi \simeq 200$. At this stage, both solutions clearly deviate from the asymptotic AMOC expression (dashed-dotted curve). At $\tau = 300$ the AMOC solution still does a very good job in the upstream region, while it deviates in the downstream region due to the growing importance of dispersion. Both solutions start to approach the asymptotic AMOC expression over the obstacle. Finally, at $\tau = 1000$, we have omitted the numerical AMOC solution, because it no longer makes sense in the far field. We notice that the Boussinesq solution agrees with the asymptotic $\eta_{bound}$ in the region $-75 < \chi < 75$, i.e. beyond the region of the obstacle. In this case the downstream undular bore is detached from the obstacle, and it gradually falls further and further behind. The toe of the leading wave of this bore follows $\eta_{bound}^{down}$ based on (4.20) very closely. The upstream undular bore is also detached, and since $\eta_{free}^{up}$ based on (4.24) is only marginally larger than $\eta_{bound}^{up}$ based on (4.20), the upstream bore resembles a uniform bore. We notice that the height of the leading soliton is approximately $H \simeq 2\eta_{free}^{up}$.

Figure 9(*a*,*b*) covers the higher-transcritical case of $\Phi = 0$ (with $L = 100$) for $\tau = 320$ and 480 respectively. With $\Phi$ being only slightly larger than $\Phi_{mid}$, the asymptotic level of $\eta_{free}^{down}$ based on (4.25) almost coincides with the bound solution $\eta_{bound}^{down}$ based on (4.20), and consequently we have omitted $\eta_{free}^{down}$ from the figure. Furthermore, since $\Phi_a^{up} < \Phi < \Phi_{high}$, we expect the upstream bore to become attached, while the downstream bore should be detached. At $\tau = 320$ the numerical AMOC solution and the Boussinesq solution both agree up to the point where dispersion becomes important. At $\tau = 480$ the numerical AMOC solution has been omitted, but we notice how the Boussinesq simulation supports the asymptotic $\eta_{bound}$ in the

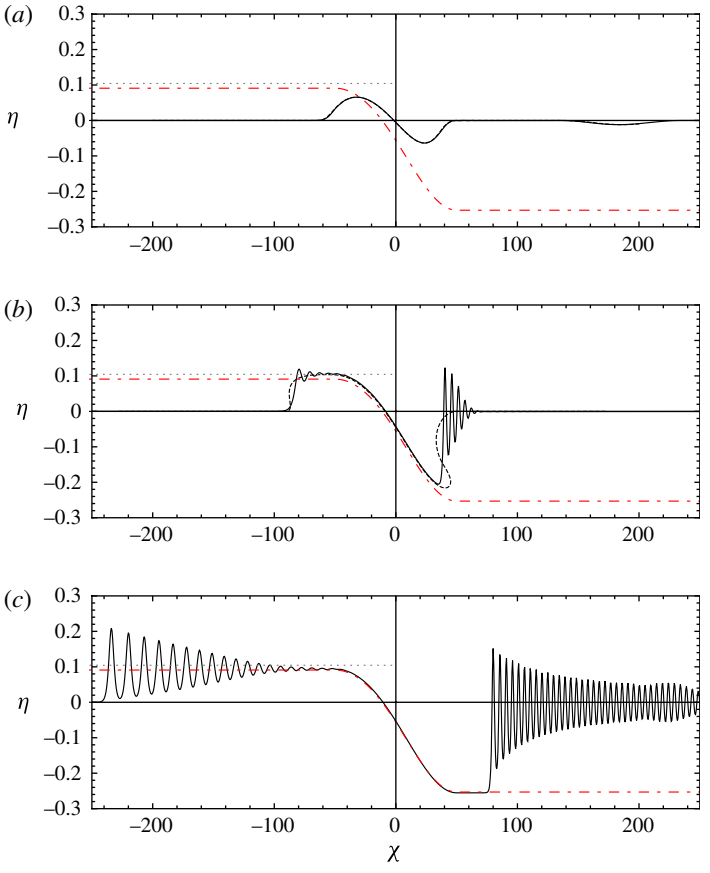


FIGURE 8. (Colour online) Snapshots, at times (*a*) $\tau = 100$, (*b*) $\tau = 300$ and (*c*) $\tau = 1000$, of the surface elevation for lower-transcritical conditions: $\Phi = -0.5$, $\Gamma_m = 0.05$ and $L = 100$. Comparison between the AMOC simulation (dashed line) and a Boussinesq simulation (full line). Dashed-dotted curve: the asymptotic level $\eta_{bound}$ based on (4.21); dotted line: the asymptotic level $\eta^{up}_{free}$ based on (4.24).

interval $-25 < \chi \leqslant 50$. The downstream bore is seen to be detached from the obstacle (as predicted), and it falls further and further behind while supporting the asymptotic level $\eta^{down}_{bound}$ based on (4.20). In contrast, the upstream bore is seen to be attached (as predicted) at approximately $\chi \simeq -30$, and this violates the AMOC solutions beyond this location. For this reason, the asymptotic AMOC solution for the upstream level overestimates the actual level, and consequently the height of the leading upstream soliton is seen to be somewhat smaller than the estimate $2\eta^{up}_{bound}$.

Figure 10(*a–c*) covers the higher-transcritical case of $\Phi = 0.5$ (with $L = 100$) for $\tau = 300$, 500 and 900 respectively. Since $\Phi^{up}_a < \Phi < \Phi_{high}$, the upstream bore is expected to be attached, while the downstream bore should be detached. Since $\Phi > \Phi_{mid}$, the leading edge of the downstream bore initially follows $\eta^{down}_{free}$ based on (4.25). In this case $\eta^{down}_{free}$ (dotted line) is clearly lower than $\eta^{down}_{bound}$ (dashed-dotted) based on (4.20). We notice that the toe of the leading downstream waves clearly follows $\eta^{down}_{free}$ at least up to $\tau = 500$. The trend is, however, that the dispersive undular bore will travel with a lower positive speed in the $(\chi, \tau)$-frame than the trough in

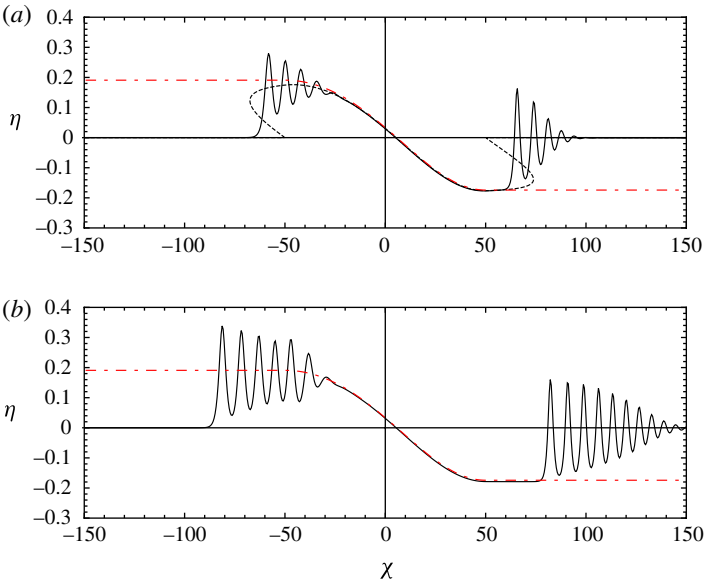


FIGURE 9. (Colour online) Snapshots, at times (*a*) $\tau = 320$ and (*b*) $\tau = 480$, of the surface elevation for transcritical conditions: $\Phi = 0$, $\Gamma_m = 0.05$ and $L = 100$. Comparison between the AMOC simulation (dashed line) and a Boussinesq simulation (full line). Dashed-dotted curve: the asymptotic level $\eta_{bound}$ based on (4.21).

the AMOC formulation, and in this process the toe of the undular bore will slowly climb the non-dispersive curve, so that the toe level gradually rises from $\eta_{free}^{down}$ to $\eta_{bound}^{down}$. This trend is clearly seen in the Boussinesq results at $\tau = 900$, where the numerical AMOC solution has been left out. As a consequence of the rising toe level, the height of the leading downstream soliton will gradually decrease, and after some time the initial influence of $\eta_{free}^{down}$ will vanish. We notice that the upstream bore is attached to the obstacle (as predicted) at $\chi \simeq -20$, and consequently the non-dispersive solutions make little sense for $\chi < -20$. Like in figure 9, this implies that the asymptotic AMOC solution for the upstream level overestimates the actual level and as a result the height of the leading upstream wave is much smaller than the estimate $2\eta_{bound}^{up}$.

Figure 11(*a–c*) covers the higher-transcritical case of $\Phi = 0.9$ (with $L = 100$) for $\tau = 400$, 600 and 1000 respectively. In the downstream region the solutions behave essentially like the previous case, and it is evident that the toe of the undular bore slowly climbs the non-dispersive curve, so that the toe level gradually rises from $\eta_{free}^{down}$ to $\eta_{bound}^{down}$. The upstream region is, however, much more extreme than in figure 10, and relatively high and steep cnoidal and solitary waves are generated close to the crest of the obstacle. This seems to influence the solution over most of the obstacle, and the Boussinesq solution only matches $\eta_{bound}$ for $\chi > 40$. Clearly, this is not a case which is suitable for non-dispersive calculations.

Figure 12 covers the supercritical case of $\Phi = 1.2$ (with $L = 50$). It shows the computed solutions for the bound wave over the obstacle and the downstream, forward-going free waves for $\tau = 100$, 200, 300 and 400. At $\tau = 100$ the agreement between the numerical AMOC solution (dashed) and the Boussinesq solution (full line) is excellent, hence dispersion clearly plays no role at this stage. Then at $\tau = 200$ dispersion starts to play a role at the leading edge of the downstream waves, and

FIGURE 10. (Colour online) Snapshots, at times (*a*) $\tau = 300$, (*b*) $\tau = 500$ and (*c*) $\tau = 900$, of the surface elevation for higher-transcritical conditions: $\Phi = 0.5$, $\Gamma_m = 0.05$ and $L = 100$. Comparison between the AMOC simulation (dashed line) and a Boussinesq simulation (full line). Dashed-dotted curve: the asymptotic level $\eta_{bound}$ based on (4.21); dotted line: the asymptotic level $\eta_{free}^{down}$ based on (4.25).

this trend further evolves at $\tau = 300$ and $\tau = 400$. Actually, the downstream forward-going free waves behave similarly to what was discussed in connection with figures 10 and 11: first of all, the lowest point of the numerical AMOC solution follows $\eta_{free}^{down}$ (dotted), while the toe of the dispersive undular bore slowly climbs the non-dispersive curve, so that the toe level gradually rises from $\eta_{free}^{down}$ to $\eta_{bound}^{down} = 0$. The bound wave over the obstacle does not change beyond $\tau = 200$, and the agreement between the non-dispersive AMOC solution and the dispersive Boussinesq solution is excellent in this region.

### 6.2. *Verification of asymptotic estimates as a function of* $\Phi$

In this section we focus on the asymptotic AMOC expressions for transcritical flow (derived in § 4.3) and for subcritical and supercritical flow (derived in § 4.4). The corresponding numerical Boussinesq solutions are of course not truly asymptotic but have been estimated on the basis of relatively long simulations.

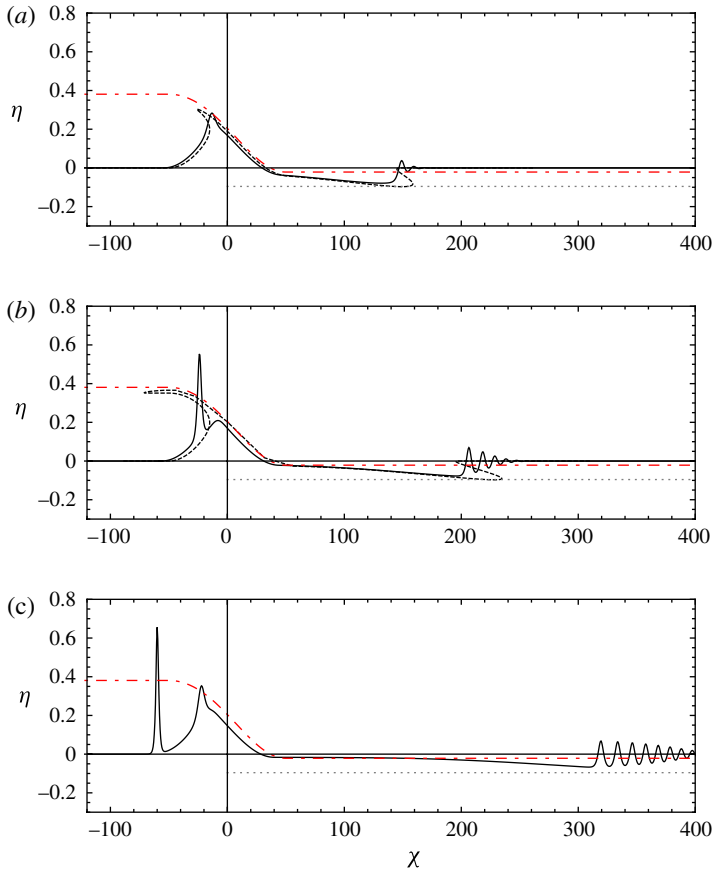


FIGURE 11. (Colour online) Snapshots, at times (*a*) $\tau = 400$, (*b*) $\tau = 600$ and (*c*) $\tau = 1000$, of the surface elevation for higher-transcritical conditions: $\Phi = 0.9$, $\Gamma_m = 0.05$ and $L = 100$. Comparison between the AMOC simulation (dashed line) and a Boussinesq simulation (full line). Dashed-dotted curve: the asymptotic level $\eta_{bound}$ based on (4.21); dotted line: the asymptotic level $\eta_{free}^{down}$ based on (4.25).

Figure 13(*a*,*b*) shows a comparison of upstream levels for the two obstacles $\Gamma_m = 0.05$ and $\Gamma_m = 0.10$, respectively. Results are shown and compared for $-1.5 < \Phi < 0$, which covers subcritical flow, lower-transcritical flow and a small part of higher-transcritical flow. It should be emphasized that the asymptotic AMOC expressions are only strictly valid as long as the upstream bore is detached from the obstacle. According to figure 5, this requires that $\Phi < \Phi_a^{up}$, i.e. less than approximately $-0.45$. This explains why the simulated values fall slightly below the theoretical estimates in the interval $\Phi_a^{up} < \Phi < 0$. For $\Phi > 0$ (not shown) the estimate of the asymptotic upstream level becomes very inaccurate because of the attachment of the upstream bore (see e.g. figure 10). First of all, figure 13 shows that the theoretical value of $\eta_{bound}^{up}$ (full line) is in excellent agreement with the Boussinesq results obtained at the upstream toe of the obstacle. Secondly, we notice that the height of the leading upstream free wave detected from the Boussinesq simulations follows the trend from the KdV estimate $H \simeq 2\eta_{free}^{up}$ (dashed line). In this connection it is remarkable that $H$ as a function of $\Phi$ varies continuously over the threshold from subcritical to

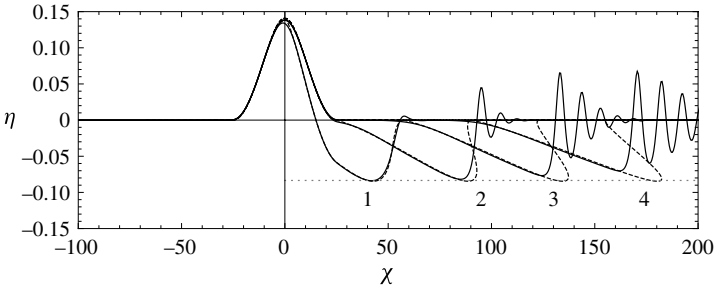


FIGURE 12. Snapshots (at four different times) of the surface elevation for supercritical conditions: $\Phi = 1.2$, $\Gamma_m = 0.05$ and $L = 50$. Comparison between the AMOC simulation (dashed line) and a Boussinesq simulation (full line). Dotted line: the asymptotic level $\eta_{free}^{down}$ based on (4.32). Snapshots shown at (1) $\tau = 100$; (2) $\tau = 200$; (3) $\tau = 300$; (4) $\tau = 400$.

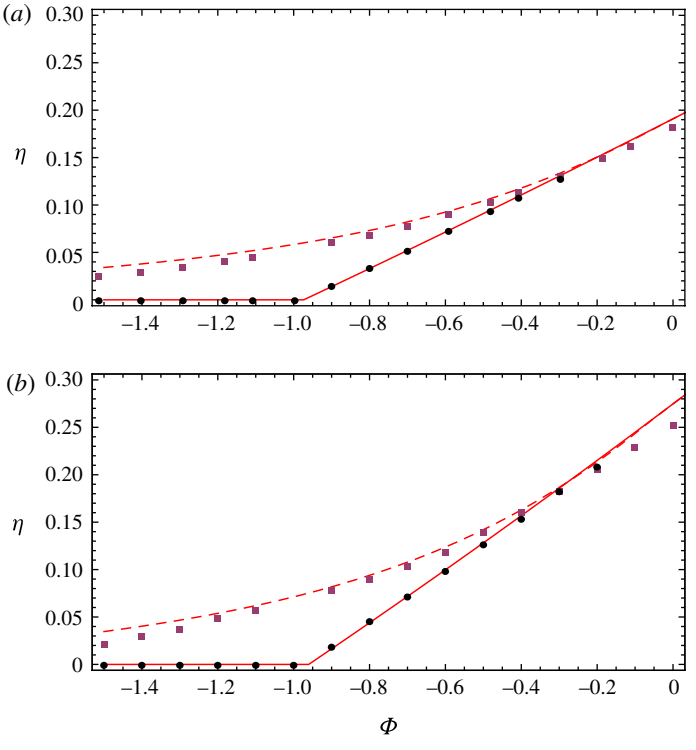


FIGURE 13. (Colour online) Asymptotic upstream levels as a function of $\Phi$ for (*a*) $\Gamma_m = 0.05$ and (*b*) $\Gamma_m = 0.10$. Full line: $\eta_{bound}^{up}$ based on (4.20); dashed line: $\eta_{free}^{up}$ based on (4.24). Boussinesq simulations: ■, half the height of the leading solitary/cnoidal waves in the upstream undular bore; •, the elevation computed at the upstream toe of the obstacle. Length of the hump: $L = 100$.

lower-transcritical flow conditions. Finally, it should be emphasized that figures 6–12 have already established that the peak of the leading edge is in excellent agreement with $\eta_{free}^{up}$ up to the point where dispersion starts to play a role. The agreement in figure 13 between $H$ and $2\eta_{free}^{up}$ is less impressive because this KdV estimate for $H$

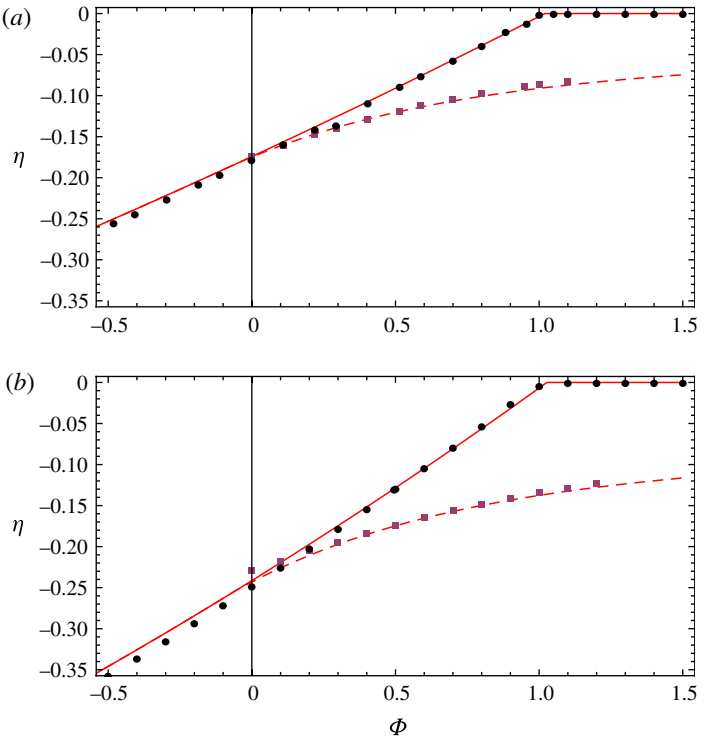


FIGURE 14. (Colour online) Asymptotic downstream levels as a function of $\Phi$ for (*a*) $\Gamma_m = 0.05$ and (*b*) $\Gamma_m = 0.10$. Full line: $\eta_{bound}^{down}$ based on (4.20); dashed line: $\eta_{free}^{down}$ based on (4.25). Boussinesq simulations: ■, half the height (shown as negative) of the leading solitary/cnoidal waves in the downstream undular bore; •, the elevation computed at the downstream toe of the obstacle. Length of the hump: $L = 100$.

tends to overestimate the wave height, and this trend increases in the subcritical domain.

Figure 14(*a*,*c*) shows a comparison of downstream levels for the two obstacles $\Gamma_m = 0.05$ and $\Gamma_m = 0.10$, respectively. Results are shown and compared for $-0.5 < \Phi < 1.5$, which covers supercritical flow, higher-transcritical flow and a small part of lower-transcritical flow. Again, it should be emphasized that the asymptotic AMOC expressions are only strictly valid as long as the downstream bore is detached from the obstacle. According to figure 5, this requires that $\Phi > \Phi_a^{down}$, i.e. larger than approximately $-0.6$. For smaller values of $\Phi$, the comparison between simulation and the asymptotic theory becomes meaningless (see e.g. figure 7). First of all, figure 14 shows that the theoretical value of $\eta_{bound}^{down}$ is in excellent agreement with the Boussinesq results obtained at the downstream toe of the obstacle, except for $\Phi < 0$ and $\Gamma_m = 0.10$. Secondly, we can again conclude that the height of the leading free wave detected from the Boussinesq simulations approximately follows the trend from the KdV estimate $H \simeq -2\eta_{free}^{down}$, and actually the agreement is better than observed in the upstream region in figure 13. Again this trend varies continuously over the threshold from higher-transcritical to supercritical flow conditions.

Figure 15 concentrates on the surface elevation obtained at $\chi = 0$, i.e. at the crest of the obstacle. In this case, results are shown and compared for the full range

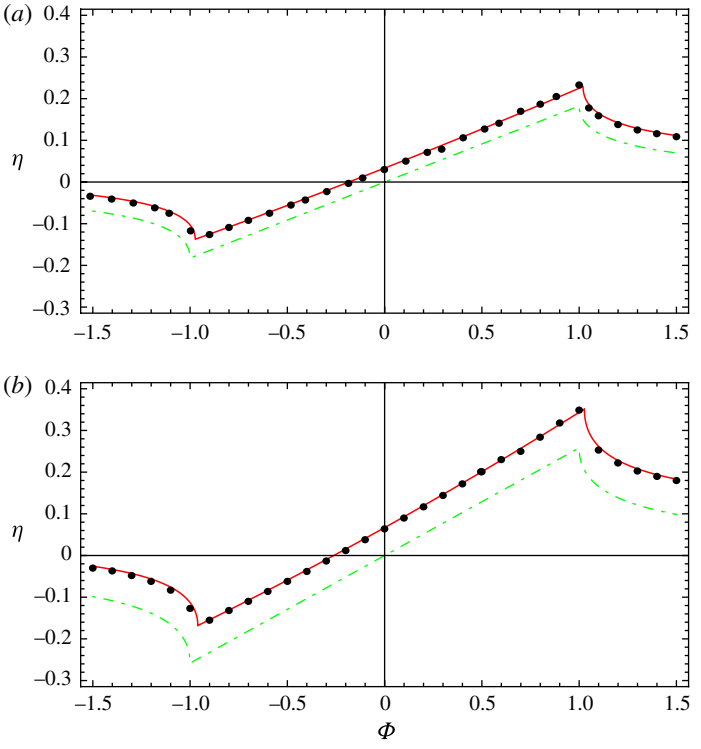


FIGURE 15. (Colour online) Asymptotic surface levels at the crest of the obstacle (i.e. at $\chi = 0$) as a function of $\Phi$ for (*a*) $\Gamma_m = 0.05$ and (*b*) $\Gamma_m = 0.10$. Full line: $\eta^{crest}_{bound}$ based on (4.23); dashed-dotted line: the Hopf solution given by (4.28); Boussinesq simulations: •. Length of the hump: $L = 100$.

of $-1.5 < \Phi < 1.5$, because the crest region is rarely influenced by the attached upstream or downstream bores. Note that $\eta^{crest}_{bound}$ obtained from (4.23) and (4.29) is in excellent agreement with the Boussinesq simulations throughout the three different flow regimes. For comparison, the dashed-dotted curve shows the corresponding Hopf solution. This solution generally underestimates the crest levels, and although the discrepancy reduces for smaller values of $\Gamma_m$ as expected, it may come as a surprise that the discrepancy is almost insensitive to the value of $\Phi$. It is, however, (3.30), i.e. $U \simeq \eta$, which is the main weakness of the Hopf solution in this connection. It does not really account for the nonlinearities occurring over the obstacle, and therefore the Hopf solution is generally poor in this region even for relatively low values of $\Gamma_m$ and $\Delta$. It should be emphasized that the Hopf solutions for the asymptotic levels at the upstream and downstream toes of the obstacle are of relatively better quality.

Figure 16 compares the computed and theoretical celerities of the leading upstream waves ($c^-_{up}$) and the leading downstream waves ($c^-_{down}$). The theoretical solution for $c^-_{up}$ is determined by (5.7) combined with $\eta_B = \eta^{up}_{free}$ based on (4.24) and (4.31), while $c^-_{down}$ is determined by (5.2) combined with $\eta_D = \eta^{down}_{free}$ based on (4.25) and (4.32). The results are shown in a fixed frame of reference, the diagonal line representing the speed of the obstacle ($V$) and the horizontal line representing the linear shallow water celerity. We notice that $c^-_{up}$ is in good agreement with the Boussinesq simulations (shown as dots) in the interval $-1.5 < \Phi < 0$, while $c^-_{down}$ is in good agreement in the

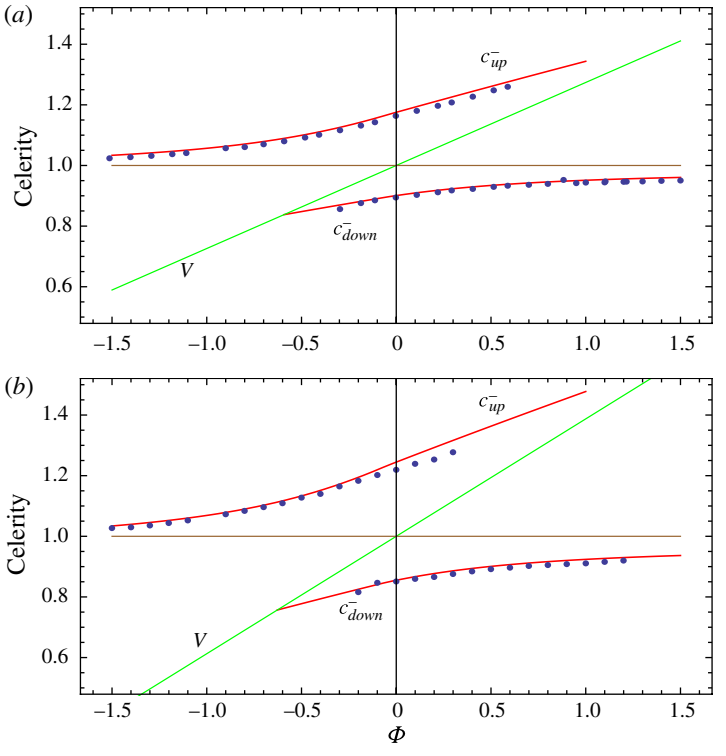


FIGURE 16. (Colour online) Fixed frame celerities of the leading edges in the upstream/downstream bores for (*a*) $\Gamma_m = 0.05$ and (*b*) $\Gamma_m = 0.10$. Full line: theoretical expressions for $c^-_{up}$ and $c^-_{down}$ based on (5.7) and (5.2). Boussinesq simulations: •. Length of the hump: $L = 100$.

interval $-0.25 < \Phi < 1.5$. The trend is, however, that the theoretical predictions are slightly on the high side compared to the simulations, and this is in agreement with the previous findings from figures 13 and 14.

## 7. Summary and conclusions

When a long, slowly varying, positive bottom obstacle of height $\Gamma_m$ is abruptly started from rest to move with a constant speed $V$, a system of transient waves will develop: free waves will propagate in the forward and backward directions, while a bound wave will settle locally over the obstacle. It turns out that in most situations, dispersion can be ignored in the vicinity of the obstacle while nonlinearity cannot. This implies that the near-field problem can be described by the NSW equations, while the far-field problem calls for Boussinesq-type equations, whenever dispersive effects become important.

Within a coordinate system moving with the obstacle, the flow conditions can be characterized as either subcritical, transcritical or supercritical and the separating thresholds are defined as $V_{low} < 1$ and $V_{high} > 1$, which are solutions to (4.14). Their variation with respect to $\Gamma_m$ is depicted in figure 3. We emphasize that, in the framework of a nonlinear formulation, critical conditions (i.e. $V = 1$) play no specific role, but it turns out to be convenient to divide the transcritical regime into a lower-transcritical and a higher-transcritical regime separated by the threshold $V_{mid}$.

This is determined by a combination of (4.18), (4.12) and (4.7), and its variation is shown in figure 3 (see also § 4.2.3). As shown by Grimshaw & Smyth (1986), the classical Hopf formulation leads to explicit expressions for $V_{low}$ and $V_{high}$, and on this basis we have chosen to classify the flow conditions in terms of a new parameter $\Phi$ defined by (4.17). This combines the effect of the height and the speed of the obstacle, and it leads to $\Phi_{low}^{Hopf} = -1$ and $\Phi_{high}^{Hopf} = 1$. On the basis of the more accurate NSW equations, $\Phi_{low}$ and $\Phi_{high}$ become weak functions of the relative height of the obstacle $\Gamma_m$, but it turns out that they do not differ much from $\pm 1$ as long as $\Gamma_m < 0.25$ (see e.g. figure 5).

The NSW equations are bidirectional and can be formulated in terms of a two-family system of characteristics (§ 3.1). This system is straightforward to solve for subcritical and supercritical conditions, but it is very difficult (if not impossible) to solve for transcritical flow, where turning points appear in the characteristic tracks. To solve this problem, we have analytically integrated and eliminated the backward-going family and achieved a versatile unidirectional single-family formulation denoted as the AMOC formulation, see §§ 3.2 and 3.3. Due to the incorporation of a memory effect, the single-family AMOC formulation accounts for the backward-going as well as the forward-going free waves, and it captures the bound solution over the obstacle with much higher accuracy than the classical Hopf formulation. While being as easy to solve as the Hopf formulation, it is (almost) as accurate as the original two-family NSW formulation. Last, but not least, the AMOC formulation is applicable not only to transcritical flow conditions, but also to subcritical and supercritical conditions. An extensive verification of the new formulation is presented in § 6.1, which covers the temporal and spatial evolution of the transient waves for a range of flow conditions. Up to the point where dispersion becomes important, the results of the AMOC formulation agree very well with numerical simulations based on a high-order Boussinesq formulation.

In § 4, we have derived an analytical asymptotic (approximate) solution to the new AMOC formulation, and this provides useful estimates of the asymptotic levels and magnitudes of the bound and free waves surrounding the obstacle. On this basis, we have discussed important concepts for transcritical flow such as turning points and the limiting characteristic (§ 4.2.1), which governs the asymptotic bound solution $\eta_{bound}$ over the obstacle including the upstream setup $\eta_{bound}^{up}$ and the downstream setdown $\eta_{bound}^{down}$. The variation of these quantities with respect to $\Phi$ has been discussed and depicted in § 6.2 and figures 13–15. Generally, these results are in very good agreement with the numerical Boussinesq simulations.

We have also discussed the importance of the crest characteristic for transcritical flow (§ 4.2.3): for lower-transcritical flow (i.e. for $\Phi_{low} < \Phi < \Phi_{mid}$), the crest characteristic governs the magnitude of the leading forward-going free wave, which propagates in the upstream region ahead of the obstacle. Expressions for the determination of $\eta_{free}^{up}$ are provided in § 4.3.1. There is a continuous transition of these expressions to subcritical flow (§ 4.4), and the variation of $\eta_{free}^{up}$ with respect to $\Phi$ (covering subcritical as well as lower-transcritical flow) has been discussed and depicted in § 6.2 and figure 13. For higher-transcritical flow (i.e. for $\Phi_{mid} < \Phi < \Phi_{high}$), the crest-characteristic initially governs the magnitude of the leading forward going free wave, which propagates in the downstream region behind the obstacle. Expressions for the determination of $\eta_{free}^{down}$ are provided in § 4.3.1. Again, there is a continuous transition of these expressions to supercritical flow (§ 4.4), and

the variation of $\eta_{free}^{down}$ with respect to $\Phi$ (covering supercritical as well as higher-transcritical flow) has been discussed and depicted in § 6.2 and figure 14.

## Acknowledgements

A. Lecoanet and C. L. Rasmussen both contributed to this work as part of their Master theses. Their efforts are acknowledged and appreciated.

## REFERENCES

BAINES, P. G. 1977 Upstream influence and Long's model in stratified flows. *J. Fluid Mech.* **82**, 147–159.

BAINES, P. G. 1984 A unified description of two-layer flow over topography. *J. Fluid Mech.* **146**, 127–167.

BAINES, P. G. 1987 Upstream blocking and airflow over mountains. *Annu. Rev. Fluid Mech.* **19**, 75–97.

BAINES, P. G. 1995 *Topographic Effects in Stratified Flows*. Cambridge University Press.

BENJAMIN, T. B. & LIGHTHILL, M. J. 1954 On cnoidal waves and bores. *Proc. R. Soc. Lond.* A **224**, 448–460.

BINNIE, A. M. & ORKNEY, J. C. 1955 Experiments on the flow of water from a reservoir through an open channel. II. The formation of hydraulic jumps. *Proc. R. Soc. Lond.* A **230**, 237–246.

COLE, S. L. 1985 Transient waves produced by flow past a bump. *Wave Motion* **7**, 579–587.

EL, G. A, GRIMSHAW, R. H. J. & SMYTH, N. F. 2006 Unsteady undular bores in fully nonlinear shallow-water theory. *Phys. Fluids* **18**, 027104.

EL, G. A, GRIMSHAW, R. H. J. & SMYTH, N. F. 2009 Transcritical shallow-water flow past topography: finite-amplitude theory. *J. Fluid Mech.* **640**, 187–214.

FAVRE, H. 1935 *Ondes de Translation*. Dunod.

FUHRMAN, D. R. & MADSEN, P. A. 2009 Tsunami generation, propagation and runup with a high-order Boussinesq model. *Coast. Engng* **56**, 467–478.

GRIMSHAW, R. & SMYTH, N. 1986 Resonant flow of a stratified fluid over topography. *J. Fluid Mech.* **169**, 429–464.

GUREVICH, A. V. & PITAEVSKII, L. P. 1974 Nonstationary structure of a collisionless shock wave. *Sov. Phys. JETP* **38**, 291–297.

HOUGHTON, D. D. & KASAHARA, A. 1968 Nonlinear shallow fluid flow over an isolated ridge. *Commun. Pure Appl. Maths* **XXI**, 1–23.

HOUGHTON, D. D. & ISAACSON, E. 1970 Mountain winds. *Stud. Numer. Anal.* **2**, 21–52.

KAMCHATNOV, A. M. 2000 *Nonlinear Periodic Waves and their Modulations*. World Scientific.

LONG, R. R. 1954 Some aspects of the flow of stratified fluids. II. Experiments with a two-fluid system. *Tellus* **6**, 97–115.

LONG, R. R. 1955 Some aspects of the flow of stratified fluids. III. Continous density gradients. *Tellus* **7**, 341–357.

LONG, R. R. 1970 Blocking effects in flow over obstacles. *Tellus* **22**, 471–480.

LONG, R. R. 1972 Finite amplitude disturbances in the flow of inviscid rotating and stratified fluids over obstacles. *Annu. Rev. Fluid Mech.* **4**, 69–92.

LONG, R. R. 1974 Some experimental observations of upstream disturbances in a two-fluid system. *Tellus* **26**, 313–317.

MADSEN, P. A., BINGHAM, H. B. & LIU, H. 2002 A new Boussinesq method for fully nonlinear waves from shallow to deep water. *J. Fluid Mech.* **462**, 1–30.

MADSEN, P. A., BINGHAM, H. B. & SCHÄFFER, H. A. 2003 Boussinesq-type formulations for fully nonlinear and extremely dispersive water waves: derivation and analysis. *Proc. R. Soc. Lond.* A **459**, 1075–1104.

MADSEN, P. A., FUHRMAN, D. R. & WANG, B. 2006 A Boussinesq-type method for fully nonlinear waves interacting with a rapidly varying bathymetry. *Coast. Engng* **53** (5–6), 487–504.

MADSEN, P. A. & SØRENSEN, O. R. 1992 A new form of the Boussinesq equations with improved linear dispersion characteristics. Part 2. A slowly-varying bathymetry. *Coast. Engng* **18**, 183–204.

MCINTYRE, M. E. 1972 On Long's hypothesis of no upstream influence in uniformly stratified or rotating flow. *J. Fluid Mech.* **52** (2), 209–243.

NWOGU, O. 1993 Alternative form of Boussinesq equations for nearshore wave propagation. *J. Waterways Port Coast. Engng ASCE* **119**, 618–638.

PEREGRINE, D. H. 1966 Calculations of the development of an undular bore. *J. Fluid Mech.* **25** (2), 321–330.

PEREGRINE, D. H. 1967 Long waves on a beach. *J. Fluid Mech.* **27**, 815–827.

PRATT, L. J. 1983 A note on nonlinear flow over obstacles. *Geophys. Astrophys. Fluid Dyn.* **24**, 63–68.

SMYTH, N. 1987 Modulation theory solution for resonant flow over topography. *Proc. R. Soc. Lond.* A **409**, 79–97.

STOKER, J. J. 1958 *Water Waves – The Mathematical Theory with Applications*. Wiley & Sons.

SU, C. H. & GARDNER, C. S. 1969 Korteweg-de Vries equation and generalisations III. Derivation of the Korteweg-de Vries equation and Burgers equation. *J. Math. Phys.* **10**, 536–539.

WHITHAM, G. B. 1974 *Linear and Nonlinear Waves*. Wiley & Sons.